ORGANOMETALLICS

Article

pubs.acs.org/Organometallics

Catalyst-Controlled Nitrene Transfer by Tuning Metal:Ligand Ratios: Insight into the Mechanisms of Chemoselectivity

Cale Weatherly,[†,§] Juliet M. Alderson,[†] John F. Berry,*[,†] Jason E. Hein,*[,‡] and Jennifer M. Schomaker*[,†]

[†]Department of Chemistry, University of Wisconsin, Madison, Wisconsin 53706, United States

[‡]Department of Chemistry, University of British Columbia, Vancouver, British Columbia, Canada V6T 1Z1

Supporting Information

ABSTRACT: Catalyst-controlled, selective nitrene transfer is often challenging when both C−H and C═C bonds are present in a substrate. Interestingly, a simple change in the Ag(I):L ratio (L = bidentate N,N-donor ligand) enables tunable, chemoselective nitrene transfer that favors either C═C bond aziridination using an ∼1:1 Ag:L ratio (AgLOTf) or insertion into a C−H bond when the Ag:L ratio in the catalyst is 1:2 (AgL_2OTf). In this paper, mechanistic studies, coupled with kinetic profiling of the entire reaction course, are employed to examine the reasons for this unusual behavior. Steady-state kinetics were found to be similar for both AgLOTf and AgL_2OTf; both complexes yield electronically similar reactive intermediates that engage in nitrene transfer involving formation of a short-lived radical intermediate and barrierless radical recombination. Taken together, experimental and computational studies point to two effects that control tunable chemoselectivity: suppression of aziridination as the steric congestion around the silver center is increased in AgL_2OTf and a decrease in the rate of C−H insertion with AgLOTf in comparison to AgL_2OTf. The observation that the sterics of Ag catalysts can be varied, with minor effects on the electronic features of the putative nitrene, has important implications for the development of other silver catalysts that enable tunable, site-selective C−H bond aminations.

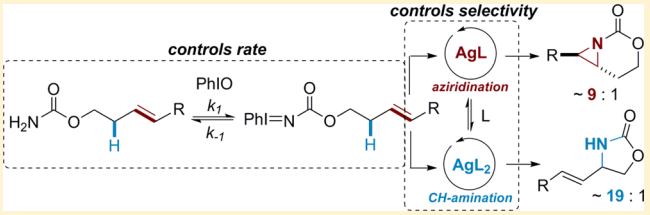

INTRODUCTION

A central challenge in contemporary catalysis is the development of methods for the oxidation of organic substrates that are *selective* for single reactive sites, operate under *catalyst-controlled* conditions (as opposed to typical substrate control), and are *tunable* for different reactive sites in a molecule.[1] Catalytic nitrene transfer comprises a powerful method to install valuable carbon−nitrogen bonds that are ubiquitous in natural products, pharmaceuticals, bioactive molecules, and ligands for catalysis.[2,3] These reactions are promoted by an array of transition metals in groups 7−11,[4−10] including dinuclear Rh(II) complexes that are typically supported by carboxylate or carboxamidate bridging ligands. These popular catalysts display high reactivity and excellent scope but tend to favor aziridination over C−H insertion when a sulfamate nitrene precursor is used in the presence of both C═C and activated C−H bonds.[3,4,10] If nitrene insertion into an allylic C−H bond is desired instead, researchers can employ dinuclear Ru catalysts containing 2-hydroxypyridine supporting ligands[12a] or porphyrin- and phthalocyanine-supported metal catalysts.[9,10,12b,c] However, few of these catalysts attain synthetically useful chemoselectivities and site selectivities in unbiased substrates with multiple, competing reactive sites,[11,12] and fewer still can be tuned to promote alternative chemoselective reactions simply through ligand modifications.

The Schomaker group has reported silver-catalyzed nitrene transfer reactions that override substrate control to achieve nondirected and tunable intramolecular aminations.[13] For example, catalysts **1** and **2**, based on AgOTf and 1,10-phenanthroline (phen) (Scheme 1), enable selective aziridination or C−H amination of homoallylic and homoallenic carbamates,[13b,c] where the reaction outcome is controlled by simply varying the ligand to AgOTf ratio. This tunability has been extended to catalysts based on electron-rich bipyridines, including **3** and **4** (*t*BuBipy).[13b] The reasons for this unexpected switch in reactivity were not clear; however,

Scheme 1. Chemoselective Ag-Catalyzed Nitrene Transfer Controlled by the Ag:Ligand Ratio

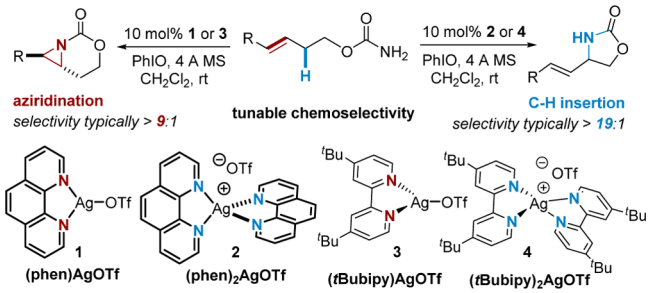

Received: March 10, 2017

DOI: 10.1021/acs.organomet.7b00190
Organometallics XXXX, XXX, XXX−XXX

resolving this issue is important to inform future efforts to expand the scope of Ag-catalyzed chemoselective and site-selective aminations. In this paper, we describe experimental and computational studies that reveal mechanistic details of the reactions in Scheme 1 by providing answers to the following questions. (1) Are catalysts **1** and **2** capable of both aziridination and C−H bond amination, and if so, how and why do the rates differ? (2) Are the silver nitrenes formed from **1** and **2** electronically similar? (3) Do reactions catalyzed by **1** and **2** proceed through similar mechanistic pathways? (4) What role does sterics play in controlling the tunable chemoselectivity?

RESULTS AND DISCUSSION

Factors That Influence the Selectivity and Mechanism of Silver-Catalyzed Nitrene Transfer. One hypothesis for the tunable chemoselectivity observed with silver catalysis is that distinct catalytic species **1** and **2** form in solution when the Ag:ligand ratio is changed. These species may have different coordination environments and/or nuclearities, leading to the observed divergence in chemoselectivity. Typical catalysts for nitrene transfer tend to display similar coordination geometries within specific classes. For example, dinuclear Rh and Ru complexes employ bridging ligands to maintain a "paddle-wheel"-type geometry in the complex,[3,4,7,11,12a] while porphyrin- and phthalocyanine-based ligands supporting monomeric Co,[9] Fe,[10] and Mn[12c] complexes also tend to have similar coordination geometries around the metal center. In contrast, silver complexes that catalyze nitrene transfer display a diverse array of coordination geometries and steric constraints in response to changes in the silver counterion, Ag:ligand ratio, solvent, temperature, and pH.[14] For example, while an ∼1:1 *t*Bubipy:AgOTf ratio yields the tricoordinate complex **3** (Scheme 1) with the OTf bound to the metal, a *t*BuBipy:AgOTf ratio of 2:1 forms the tetracoordinate **4** with an outer-sphere OTf.[14a,h] Other Ag:bipyridine ratios furnish dimeric and oligomeric structures[14a,i] influenced by the nature of the solvent, counterion, and stoichiometry.[14] Though limited analogies can be drawn between solid-state and solution behaviors, these examples attest to the diversity of potential bonding modes and nuclearities available to Ag(I) complexes. Thus, correlations of the solution-state structure of the resting state of Ag catalysts might be helpful to understand tunable chemoselectivity.

A second possible reason for the observed tunable chemoselectivity is the existence of different mechanisms of nitrene transfer for either the mono- or bis-ligated species (Scheme 1, **1** vs **2** and **3** vs **4**). Two general mechanistic schemes for intramolecular metal-catalyzed nitrene transfer tend to be observed among diverse catalyst systems (Scheme 2),[15] with the basic features proposed in Kwart's seminal report on Cu-promoted decomposition of a sulfonyl azide.[16] Reaction of a nitrogen transfer reagent with an oxidant, such as PhIO, generates the imidoiodinane **6**, which is then transferred to the metal to generate a metal−supported nitrene of the form **7** or **8**. Variations in this general mechanistic scheme are often attributed to differences in the electronic structures of the metal nitrene intermediates.[15f,i,k,17,18] These differences are often presented as a simple binary scheme, wherein triplet metal nitrenes **8** promote stepwise amination either through stepwise addition of the nitrene to an alkene or by an H atom abstraction/radical recombination process, while singlet metal nitrenes **7** carry out concerted, asynchronous amination by

Scheme 2. General Mechanisms of Metal-Catalyzed Nitrene Transfer

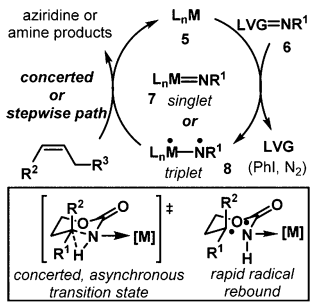

Experiment	L_nM=NR *singlet nitrene*	$L_n\dot{M}$-$\dot{N}$R *triplet nitrene*
	Expected outcome	
allylic amination	no *E*:*Z* isomerization	isomerization
radical inhibitors	no change	yield decreases
radical clock	lack of rearrangement	olefin formation
Hammett	negative ρ value linear plot	concavity/ break in plot
Intrinsic KIE	1.1-4.0	> 4.0

insertion into a reactive C−H or C=C bond (Scheme 2, left). While there are examples where this paradigm does not apply, it is worth considering as a potential reason for the bifurcated reactivity observed in our silver catalyst systems.

Common experimental probes of these competing mechanistic pathways (Scheme 2, right) include isomerization of alkene geometry, ring opening of radical clocks, the effects of radical inhibitors, linear free energy relationship studies of styrene aziridination and benzylic C−H insertion, and the measurement of intrinsic kinetic isotope effects (KIE). Within this mechanistic paradigm, the divergence in chemoselectivity displayed by the two Ag complexes can be attributed to electronically distinct nitrenes, each with a unique propensity toward *either* aziridination *or* C−H amination.

A final proposal for our tunable chemoselectivity is that the mono- and bis-ligated Ag complexes support nitrenes with the same electronic structure, but the different steric environments enforce divergent reaction pathways. In this scenario, both catalysts favor similar mechanisms for the nitrene transfer event but display *different* reaction *rates* for aziridination vs C−H insertion. This is an intriguing scenario, but few detailed kinetic studies of catalytic nitrene transfer reactions have been reported. Jacobsen and co-workers obtained evidence for ligand acceleration in Cu-catalyzed aziridination,[15l] while Chang observed a second-order dependence on the copper catalyst in aziridinations with 2-pyridylsulfonyl moieties.[15m] In other selected studies, Du Bois' initial rate kinetic studies of Rh_2-dicarboxylate catalysts revealed zero-order rate dependence on the catalyst,[15j] while Warren's stoichiometric kinetic study of Cu nitrenes demonstrated an inverse dependence on added Cu, a crucial piece of evidence supporting a pre-equilibrium between Cu dimer nitrenes and the catalytically active monomeric Cu nitrene intermediate.[15i] To achieve a better understanding of our silver systems, including catalyst activation, deactivation, product inhibition, and maximum reaction rates, we undertook a closer examination of the kinetic details of Ag-catalyzed nitrene transfer. Insight from these studies can aid the development of more active and selective catalysts and furnish standard design principles applicable to other types of metal-catalyzed, chemoselective oxidation protocols.

Dynamic Behavior of Ag(I) Complexes in Solution. The effect of the AgOTf:ligand ratio on the population distribution of Ag species in solution has been previously explored by carrying out NMR studies at various AgOTf:*t*Bu-Bipy ratios.[13b] AgOTf was dissolved in CD_2Cl_2 and the ligand added in 0.5 equiv portions up to 5.0 equiv ligand/equiv of AgOTf. Unfortunately, the rapid rate of ligand exchange, even at −80 °C, prevented the observation of discrete silver species

DOI: 10.1021/acs.organomet.7b00190
Organometallics XXXX, XXX, XXX−XXX

by ^{1}H NMR spectroscopy. Efforts to isolate authentic samples of **1** and **2** directly resulted only in the recovery of **2**; however, indirect evidence for dynamic exchange between **1** and **2** could be obtained (Scheme 3).[13b] When **9** was treated with the

Scheme 3. Indirect Evidence for the Dynamic Behavior of Silver Catalysts for Nitrene Transfer

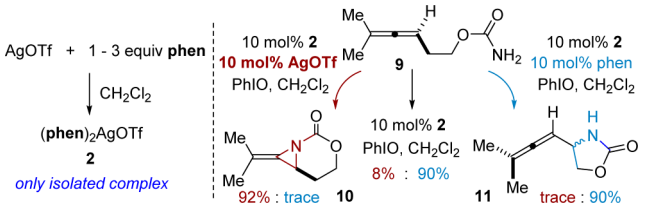

isolated complex **2** or with additional ligand, C−H bond amination dominated to yield mainly **11**. In contrast, when **9** was treated with both **2** and added AgOTf, the reaction selectively gave aziridine **10**.

Dynamic ligand exchange with a bidentate nitrogenated ligand can also favor dimeric or oligomeric Ag ligand clusters. In their report on Ag-catalyzed aziridination, He and coworkers obtained crystals of a disilver(I) complex and posited this dimer as the active catalyst.[5a] Given this and the many precedents for the existence of multinuclear Ag species in the solid state,[14] we considered that one or both of our active catalysts might consist of dimers or higher aggregates, allowing metal−metal interactions to play a central role in the observed catalytic activity. DOSY-NMR aided in ascertaining the nuclearity of the Ag complexes in solution. To improve solubility, phen was replaced with a *t*BuBipy ligand, which displayed tunable chemoselectivities similar to those observed with phen. DOSY indicated that the primary resting state of the complex in solution at a 1:1.25 AgOTf:*t*BuBipy ligand loading (0.05 M) is monomeric Ag(*t*BuBipy)OTf, while higher ligand loadings of up to 1:3 AgOTf:*t*BuBipy resulted in the formation of Ag(*t*BuBipy)$_2$OTf (Scheme 1, **3** and **4**, respectively).[13b] Addition of the PhIO oxidant did not affect the nuclearity of either complex; both remained monomeric in solution. While the possibility of Ag···Ag interactions in the reactive nitrene intermediate cannot be ruled out, it appears that monomeric Ag complexes with different coordination numbers are the most likely species responsible for both nitrene transfer pathways.

Probing the Nature of the Metal Nitrene Intermediates. Differences in the electronic structure of the putative nitrenes bound to the Ag atom in **3** and **4** might account for differences in chemoselectivity, perhaps by promoting concerted vs stepwise nitrene transfer. Physical organic experiments can help to elucidate the relationship among catalyst composition, silver nitrene electronic structure, and the observed chemoselectivity. However, there are caveats in that mechanisms involving short-lived radical intermediates cannot always be ruled out using experimental studies; in these cases, computational studies are valuable for obtaining further insight into reaction pathways (vide infra).[12a,b,15h,j,17−19] Nonetheless, independent reactions with **12**-*Z* or **12**-*E* yielded a single stereoisomer of the expected products on treatment with standard aziridination or C−H amination conditions (Scheme 4, top).[13b] Only *cis*-**13a** was obtained from **12**-*Z*, while only the *trans*-aziridine **13c** was observed in the reaction of **12**-*E* under both sets of reaction conditions. In the C−H amination pathway, the stereochemical probes **14a,c** were treated with 1:3

Scheme 4. Isomerization and Stereochemical Probes for Nitrene Transfer

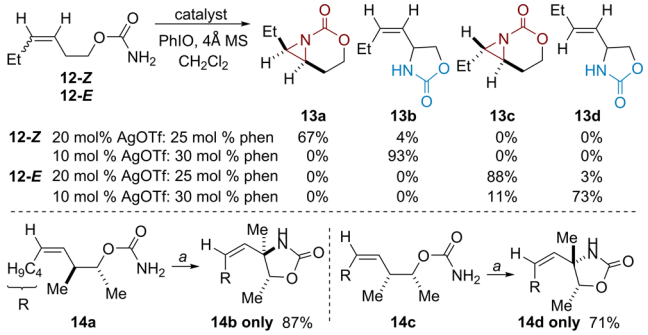

AgOTf:*t*BuBipy under typical reaction conditions. Both substrates gave only a single diastereomer of the product, with no evidence for isomerization (Scheme 4, bottom).[1g,13b,15n]

Isomerization in the reactions reported in Scheme 4 would have provided support for a stepwise mechanism, but the observed retention of stereochemistry does not rule out a rapid radical rebound pathway. Evans and Perez have demonstrated that isomerization in stepwise aziridination processes can be highly substrate dependent;[8b,15h] however, in our case, the observed retention of stereochemistry under conditions that select for either aziridination or C−H bond amination suggests that both pathways are likely to proceed from electronically similar metal nitrene complexes, whatever the actual mechanism may be.

The possibility of radical intermediates was further assessed through reactions of **15** (Scheme 5, top) in the presence of

Scheme 5. Effect of Radical Inhibitors and Traps on the Chemoselectivity

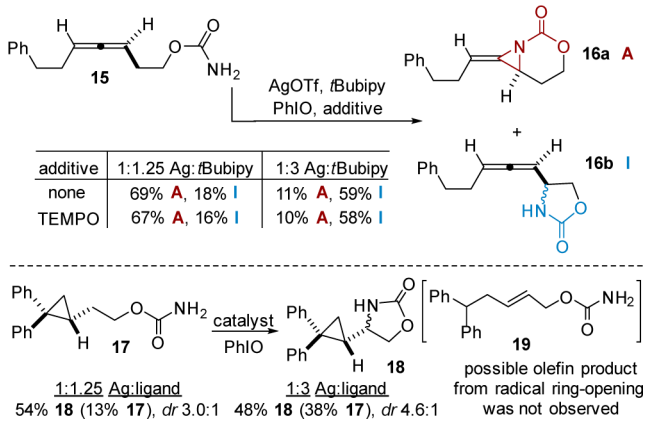

equimolar amounts of catalyst and the radical inhibitor TEMPO (2,2,6,6-tetramethylpiperidine-1-oxy radical). Radical inhibitors with exchangeable protons, such as BHT (2,6-di-*tert*-butyl-4-methylphenol), do affect the rate of nitrene transfer, but their ability to perturb the equilibrium between AgLOTf and AgL$_2$OTf leads to uncertainty as to whether this effect is due to stepwise nitrene transfer.[13b] The differences between the yields obtained under both sets of conditions were within experimental error, indicating that, if radical intermediates are formed, they have lifetimes too short to be intercepted by these inhibitors. Silver-catalyzed nitrene transfer in the presence of **17**

DOI: 10.1021/acs.organomet.7b00190
Organometallics XXXX, XXX, XXX−XXX

bearing an intramolecular radical trap (Scheme 5, bottom) was also carried out. The putative radical generated from this substrate should undergo cyclopropane ring opening with a rate of approximately 4×10^{11} s^{-1}.[20] Performing the reaction under conditions of both high and low Ag:ligand loadings gave only **18** as the product, along with remaining **17**. No olefin product **19**, indicative of cyclopropane ring opening, was noted in either reaction.

Intramolecular competition experiments using differentially substituted bis-aryl carbamates **20a−e** (Scheme 6)[21] were

Scheme 6. Hammett Studies of Ag-Catalyzed C−H Amination

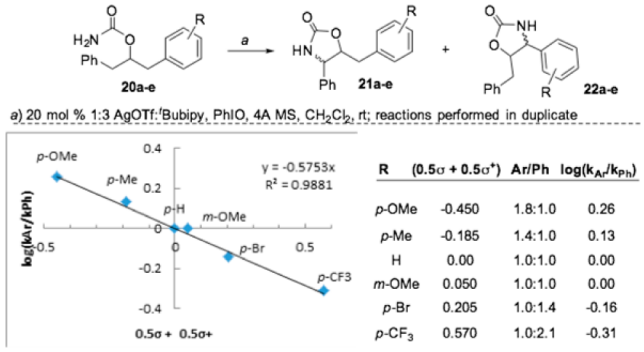

R	(0.5σ + 0.5σ⁺)	Ar/Ph	log(k_{Ar}/k_{Ph})
p-OMe	-0.450	1.8:1.0	0.26
p-Me	-0.185	1.4:1.0	0.13
H	0.00	1.0:1.0	0.00
m-OMe	0.050	1.0:1.0	0.00
p-Br	0.205	1.0:1.4	-0.16
p-CF_3	0.570	1.0:2.1	-0.31

conducted, using analysis of the resulting mixtures of **21a−e** and **22a−e** to infer differences in C−H amination rates. When a 1:3 Ag:ligand ratio was employed, a linear correlation was obtained using an equally weighted average of σ and σ^+ parameters.[22] Parameters that quantify radical involvement in benzylic C−H functionalization, such as Jiang's spin delocalization constants, did not account for the strongly deactivating effect of the *p*-CF_3 group.[23] The linear free energy correlation revealed a ρ value of −0.58,[24] which is consistent with moderate positive charge buildup in the transition state during C−H amination and would be expected for a concerted, asynchronous process with a relatively early transition state. A similar ρ value of −0.55 was obtained by Du Bois and co-workers in their examination of Rh-catalyzed nitrene transfer, which has also been attributed to concerted addition of a singlet metal-nitrene.[15j,1g] An identical ρ value of −0.58 was obtained when a 1:1.25 Ag:ligand ratio was employed (see Figure S1 in the Supporting Information for complete details). However, the possibility of a stepwise pathway still cannot be completely ruled out, as these do not always result in Hammett plots displaying concavity or nonlinear correlations.[12a,c] Nonetheless, our experimental results again point to similar electronic behavior between nitrenes formed from AgLOTf and AgL_2OTf.

Computational Studies of Putative Nitrene Intermediates. Silver nitrene species have been extensively examined computationally by Pérez[15h] and by us in previous work.[25] Related studies of copper nitrenes are also germane to our work.[26] The results of DFT and higher-level ab initio (CASSCF) calculations implicate a triplet ground state for silver nitrene species.[25] In Rh_2-catalyzed reactions, the viability of a concerted mechanism has been traced to the requirement for an empty N-centered orbital in the metal nitrene intermediate, a requirement that is likely to be general and thus necessitates a low-spin state.[18b] In contrast to Rh_2 complexes, the electronic structure of the silver nitrene does not provide the empty N-centered orbitals necessary to facilitate aziridination or C−H amination via a concerted mechanism (see Chart 1). Aziridination and C−H amination

Chart 1. Comparison of the Electronic Structures of Rh_2- and Ag-Nitrene Species

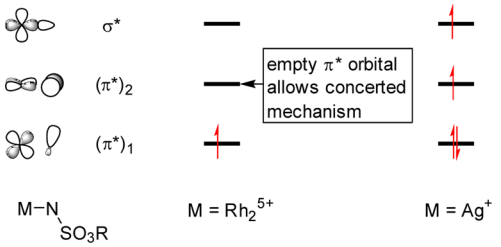

mechanisms are therefore necessarily stepwise; however, Perez has shown in the case of aziridination,[15h] and we have shown in the case of C−H amination,[25] that the recombination step can occur without a barrier (i.e., radical species are not necessarily stationary points on the potential energy surface). In the case of C−H amination, a hydrogen atom transfer (HAT) transition state is followed either by direct formation of products (barrierless recombination) or by radical intermediates, with different silver catalysts leading to different intermediate lifetimes.[26] The strength of the Ag−N bond in the nitrene complex was important in distinguishing between complexes that undergo barrierless vs nonbarrierless radical recombinations. For example, a bidentate N,O-coordination mode for a sulfamate-derived nitrene, similar to the proposed coordination mode in a metastable copper nitrene complex described by Ray and co-workers, leads to a barrierless radical recombination.[26a]

To provide computational insight into differences in the electronic structures of nitrenes formed with differing Ag:ligand ratios, nitrenes modeled on Ag(I) precursors **3** and **4** (Figure 1a) were studied. Density functional theory (DFT) methods were used throughout, as we found these to be successful in previous work and were consistent with the results of higher-level CASSCF calculations.[25] Optimized catalyst structures were based on the crystallographic data[27,28] for Ag(*t*BuBipy)OTf (**3**) or Ag(*t*BuBipy)$_2$OTf (**4**) and used with the simplified nitrene precursor **23**. Imidoiodinane **23** adducts of **3** and **4** were optimized to Ag(*t*BuBipy)(OTf)(imidoiodinane) (**24a**, not shown) and [Ag(*t*BuBipy)$_2$(imidoiodinane)]OTf (**25a**, not shown). Dissociation of PhI from these two intermediates gave the complexes Ag(*t*BuBipy)(OTf) (nitrene) (**24b**) and [Ag(*t*BuBipy)$_2$(nitrene)]$^+$ (**25b**). Both structures were examined using a relaxed surface scan that elongated the N−I bond distance from the normal bond distance of ∼2.1 Å to a nonbonding distance of ∼5 Å. The transformation **24a** → **24b** + PhI has ΔG = +13.0 kcal/mol, while **25a** → **25b** + PhI with ΔG = +8.2 kcal/mol is more facile, as expected on the basis of steric differences. Both processes are essentially barrierless.

Experimental support for the proposed intermediates **24b** and **25b** was obtained by carrying out chemoselective amination studies with a variety of different silver salts. If the silver counteranion is bound to the metal under conditions favoring aziridination, its identity is expected to influence the chemoselectivity of the nitrene transfer. In contrast, the selectivity under conditions favoring C−H amination should show less of a response to the anion identity. Experiments (Table S6 in the Supporting Information) supported this hypothesis, as aziridination at low ligand loadings was completely diverted to C−H amination when the silver

DOI: 10.1021/acs.organomet.7b00190
Organometallics XXXX, XXX, XXX−XXX

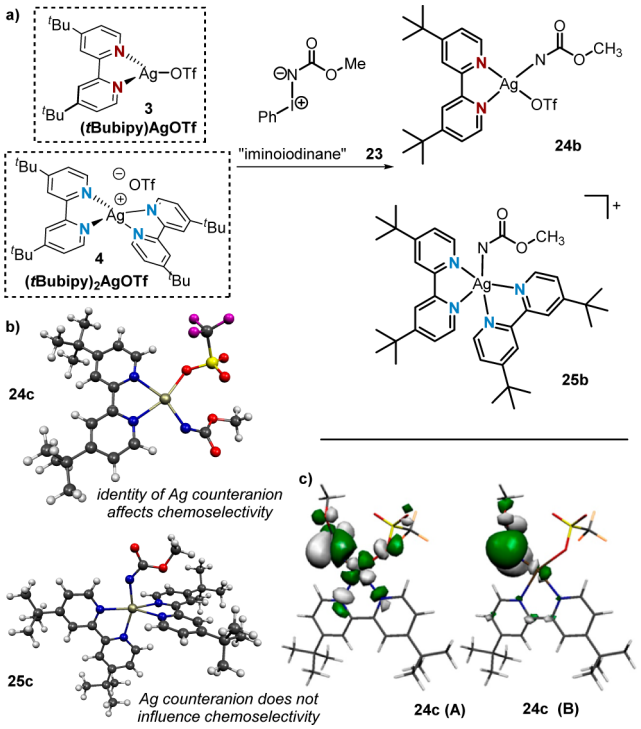

Figure 1. (a) Structures employed in DFT calculations. (b) Drawings and optimized structures of **24c** and **25c**. (c) SOMOs of **24c** having Ag–N σ^* (A) and π^* (B) symmetry.

counteranion was changed from OTf to OAc. On the other hand, C–H amination was preferred at high ligand loadings, irrespective of the identity of the silver salt.

The optimized, truncated structures of **24b** and **25b**, labeled as **24c** and **25c**, are shown in Figure 1b. Compound **24c** is nearly square planar, whereas **25c** is close to a square-pyramidal structure (τ = 0.2) with one of the bipy N atoms in the apical position. Since pure DFT functionals such as BP86 are well-known to have an intrinsic bias toward low-spin configurations,[15h,29−32] the electronic structures of **24c** and **25c** were calculated using the hybrid functional B3LYP. With B3LYP, the ground states of both **24c** and **25c** are spin triplets, S = 1, favored by 9.3 and 8.1 kcal/mol, respectively. The electronic structures of **24c** and **25c** are nearly identical; the two unpaired electrons reside in orbitals of σ^* and π^* symmetry with respect to the Ag–N bond. The representative SOMOs for **24c** are shown in Figure 1c. The similar electronic structures of **24c** and **25c** suggest that the differences in their reactivity may be steric in nature, rather than electronic. These results, in agreement with the experimental data reported herein and our previous computational investigations,[15h,25] suggest stepwise aziridination/C–H amination pathways occurring via barrierless radical recombination, such that no radical intermediates are observable or interceptable in the reaction.

Kinetic Studies of Ag-Catalyzed Aziridination and C–H Bond Amination. While our experimental and computational studies thus far suggested that nitrenes generated from AgLOTf and AgL_2OTf are electronically similar, further kinetic analyses were necessary to provide a more comprehensive mechanistic picture of the factors controlling catalytic pathways promoted by the two different silver species. Few detailed kinetic investigations have been reported for nitrene transfer reactions, and the bulk of these focus on initial rate analysis.[15i,j,l,m] We felt such treatment of our system was not suitable, as preliminary kinetic studies indicated significant nonideal behavior, including acceleration in the reaction rate after initiation that required 20–30 min to reach a steady state. A combination of factors could be responsible for this nonideal behavior, including catalyst activation, substrate inhibition, or potential mass transfer limitations due to the low solubility of the PhIO oxidant. In addition, the dynamic and fluxional nature of the Ag:ligand complex, coupled to the array of potential equilibria, seriously complicates kinetic analysis using only initial rate measurements. An alternative approach involves acquiring the entire reaction profile and interpreting these data using kinetic analysis by employing RPKA[33a] or kinetic profiling[33b,c] to assess complex kinetic behavior in this nonideal system. Reaction progress analyses were carried out by periodically removing aliquots from reaction mixtures and sampling by HPLC, with independent analyses of five early aliquots by ^{1}H NMR to cross-validate the HPLC method.

Reaction profiles were first obtained with 10 mol % AgOTf under standard aziridination (Figure 2A, reaction A, 12.5 mol % ligand) and C–H amination conditions (reaction B, 30 mol % ligand). One immediately apparent difference between the two reaction conditions was a 20–25 min induction period when less ligand (12.5 vs 30 mol %) was employed. The trends for carbamate **15** consumption were directly compared by

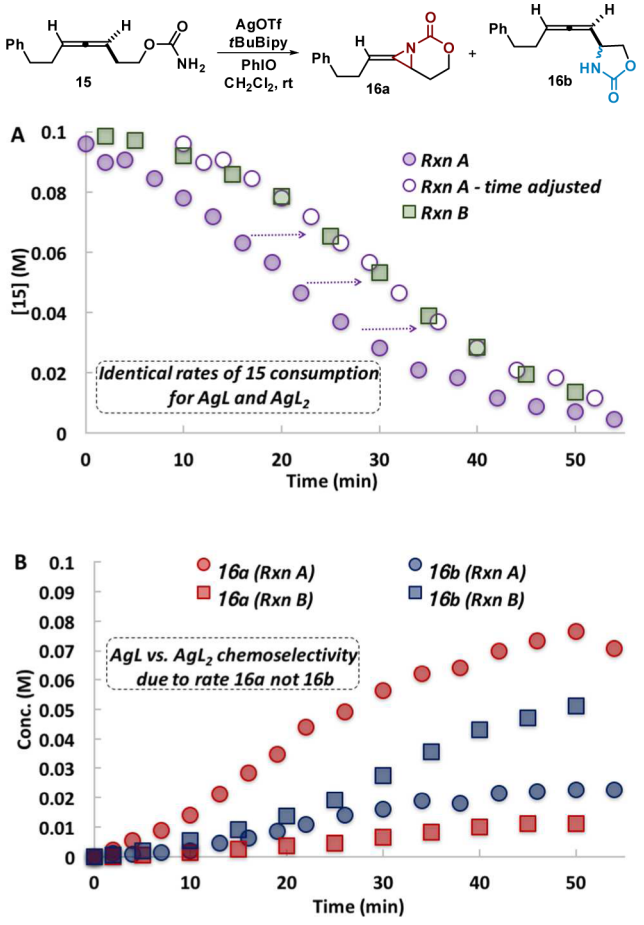

Figure 2. Reaction profiles showing (A) consumption of **15** with either *t*BuBipyAgOTf (reaction A) or $(t\text{BuBipy})_2$AgOTf (reaction B) and (B) formation of **16a,b** over time for both reaction A and reaction B conditions. Conditions: reaction A, 0.1 M **15** in CH_2Cl_2, 10 mol % AgOTf, 12.5 mol % *t*BuBipy; reaction B, 0.1 M **15** in CH_2Cl_2, 10 mol % AgOTf, 30 mol % *t*BuBipy.

DOI: 10.1021/acs.organomet.7b00190
Organometallics XXXX, XXX, XXX–XXX

adjusting the time offset from reaction A to compensate for the induction period. This analysis reveals that, despite the differences in initial activity, both reactions display nearly identical rates of substrate consumption once a steady state is reached. Examination of the trends for product formation (Figure 2B) highlights the observed switch in chemoselectivity, with **16a** being generated faster at a lower ligand loading (reaction A) and **16b** being favored with excess ligand (reaction B). Curiously, the rates of C−H amination to give **16b** are quite similar for both reactions, especially in the initial stages; in contrast, the rate of aziridination is markedly depressed when higher ligand concentrations are used. This result illustrates that, while the rates of carbamate consumption are identical, regardless of the ligand environment of the catalyst, there is a marked switch in the chemoselectivity.

The relationship between chemoselectivity and ligand concentration was further explored (Figure 3). Increasing the

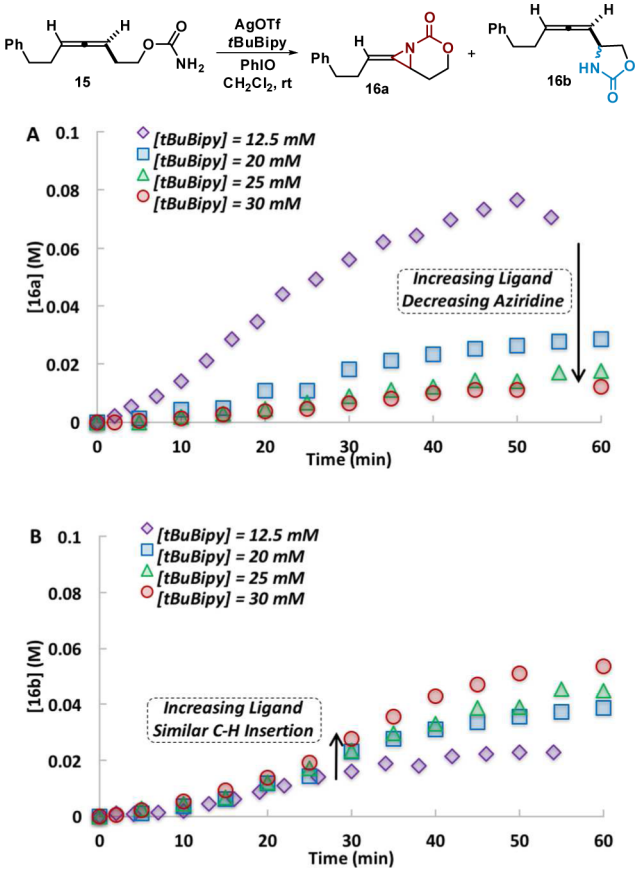

Figure 3. Product formation for varied *t*BuBipy ligand loadings: (A) reaction profiles for **16a** with [*t*BuBipy] from 12.5 mM to 30 mM; (B) reaction profiles for **16b** with [*t*BuBipy] from 12.5 mM to 30 mM. Reaction conditions: 0.10 M **15** in CH_2Cl_2, 0.010 M AgOTf, powdered 4 Å MS (1 g/mmol **15**), indicated mM of *t*BuBipy.

concentration of *t*Bubipy from 12.5 mM (12.5 mol %) to 30 mM (30 mol %) resulted in a progressive and substantial decrease in the rate of aziridination (Figure 3A). In contrast, the rate of C−H amination (Figure 3B) is less affected as the amount of *t*Bubipy increases, suggesting that the formation of **16b** displays a pseudo-zero-order dependence on catalyst concentration. Thus, it appears the observed change in chemoselectivity from aziridination to C−H insertion is a consequence of *suppressing* the formation of **16a**, as opposed to *accelerating* the generation of **16b**.

Investigations of the ability of Ag(*t*Bubipy)$_2$OTf **4** to promote aziridination when a C−H amination pathway is not available, as well as the parallel ability of Ag(*t*Bubipy)OTf **3** to catalyze C−H amination in the absence of an alkene functionality, were carried out. The allylic C−H bonds of **26** (Scheme 7) were replaced with Me groups to block C−H

Scheme 7. Comparison of AgLOTf and AgL$_2$OTf Catalysts[a]

catalyst	*t*Bubipy	yield (*dr* **27a:27b**)	init. rate (M/min)[a]
3	12.5 mol%	65% (**16**:1)	2.62×10^{-3}
4	30 mol%	63% (**13**:1)	1.35×10^{-3}

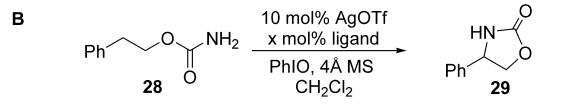

catalyst	*t*Bubipy	yield **29**	init. rate (M/min)[a]
3	12.5 mol%	44%	1.25×10^{-3}
4	30 mol%	54%	1.71×10^{-3}

[a]The rate of product formation was monitored by ^{1}H NMR with mesitylene as the internal standard. Initial rates are the average of two runs.

insertion. Similar yields and dr values of the aziridine products **27a:27b** were observed with both **3** and **4** (Scheme 7A). Initial rates were determined, corresponding to the rates of consumption of **26** and **28** after the system had reached a steady state (see the Supporting Information for further details). Interestingly, the initial rate of aziridine formation (**27a,b**) using **3** was almost double the rate using **4**. This result suggests that, while both **3** and **4** are able to promote aziridination, the sterically restricted environment around the metal center in **4** results in lower observed rates of cyclization. Furthermore, this effect is exacerbated in bulky homoallenic carbamates, as we have reported in our previous work.[13b]

Studies with **28** (Scheme 7B) revealed that the rate of C−H insertion using either AgLOTf **3** or AgL$_2$OTf **4** are very similar. This result mirrors our findings, which show that the rate of C−H amination is largely insensitive to the metal:ligand ratio. This implies that the C−H amination pathway displays little dependence on the catalyst concentration, regardless of whether AgLOTf or AgL$_2$OTf is the dominant complex. Taken together, these experiments show that catalyst sterics significantly affect the chemoselectivity of nitrene transfer. Bulky homoallenic carbamates are affected to a greater degree than less sterically hindered homoallylic carbamates; both systems show differences in the initial rates of aziridination and C−H insertion, depending on the catalyst identity.[13b]

The effect of varying catalyst loadings, while a constant AgOTf:ligand ratio of either 1:1.25 or 1:3 was maintained, was investigated (see Figures S16 and S17 in the Supporting Information for details). Interestingly, the **16a:16b** ratios for both the 1:1.25 and 1:3 AgOTf:ligand systems remained nearly constant across catalyst loadings, confirming that the chemoselectivity is related to the ligand environment at Ag(I), rather than the absolute concentration of the metal.

DOI: 10.1021/acs.organomet.7b00190
Organometallics XXXX, XXX, XXX−XXX

While it was apparent that the rate of carbamate consumption is proportional to either AgLOTf **3** or AgL_2OTf **4**, it is difficult to extract the exact numerical relationship, as the catalyst induction period results in reaction progress curves that are not readily interpreted by initial rate analysis. In such cases, we can apply a graphical analytical method, whereby the time axis is adjusted to "normalize" the impact of different catalyst concentrations on the reaction profile.[34] This powerful technique allows the order in catalyst (n) to be extracted without solving the exact function describing the reaction profile. For these data, graphical analysis reveals good agreement in reaction trends when [**15**] is plotted against time × $[AgOTf]^n$, where n = 0.5 (Figure 4). An observed

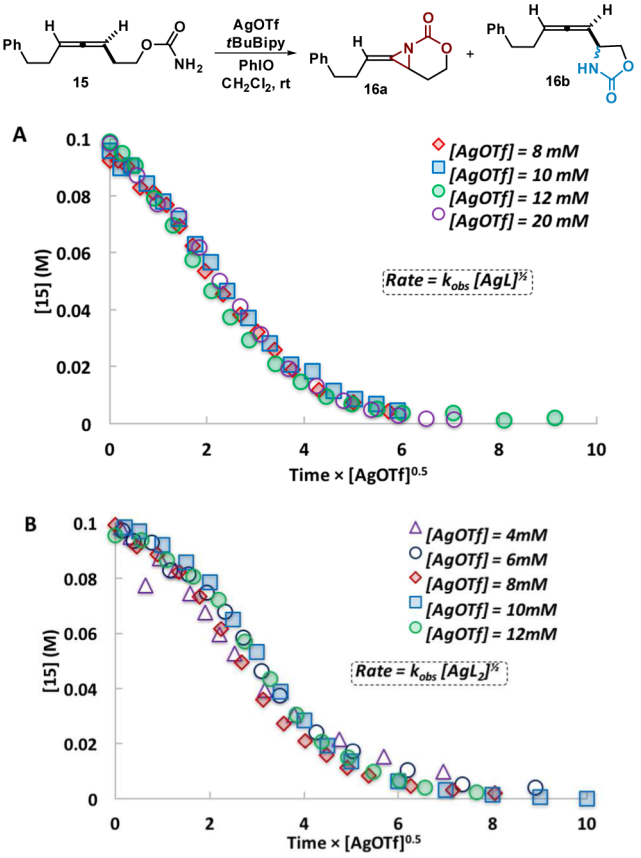

Figure 4. Consumption of **15** at varied catalyst concentrations while maintaining a 1:1.25 AgOTf:ligand ratio (A) or a 1:3 AgOTf:ligand ratio (B). Both graphs are normalized.

fractional order in catalyst suggests that the metal complex exists partly as an off-cycle, unreactive dimer or oligomer. Similar behavior has been reported for Pd-catalyzed Heck coupling, where the formation of an inactive dimeric complex in fast equilibrium with the active monomeric species leads to the observation of fractional order in palladium.[35] Thus, the silver may be distributed among three main pools (Figure 5): monoligated AgL that preferentially catalyzes aziridination, a bis-ligated AgL_2 species that leads to C−H amination, and higher-order aggregates $(Ag_xL_y)_n$ that are unreactive. This model explains the observed ligand-dependent chemoselectivity. By keeping the ligand concentration low, the system favors mainly the monoligated AgL, but the addition of excess ligand tends to populate both the bis-ligated AgL_2 and oligomeric complexes, while depleting the AgL reservoir. In addition, this

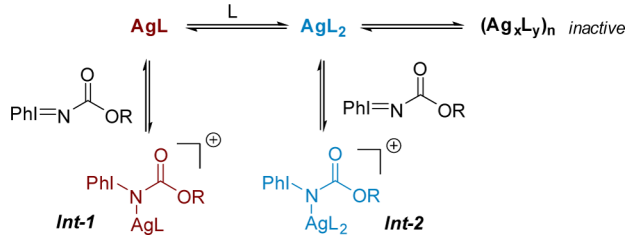

Figure 5. Partitioning of silver complexes in nitrene transfer.

model allows the concentration of the bis-ligated AgL_2 complex to remain fairly constant over a range of ligand concentrations, leading to the observed invariance in the C−H bond amination rate with varied ligand concentration.

Varying the initial concentration of carbamate **15** had little effect on the reaction rate, regardless of the Ag:ligand ratio. This suggests that either dissolution of insoluble PhIO or reaction to form the key imidoiodinane intermediate represents the turnover-limiting step for the aziridination and C−H amination processes. While the overall reaction rate is relatively insensitive to the initial concentration of **15**, a small perturbation in chemoselectivity was observed. When a 1:1.25 Ag:ligand ratio was used, the aziridination rate remained constant; however, C−H amination increased, altering the final **16a**:**16b** ratio from 5.3:1 to 2.5:1 (Figure 6A, $[15]_0$ = 0.08−0.12 M). In contrast, the initial concentration of **15** had no effect on the reaction profile for either aziridination or C−H

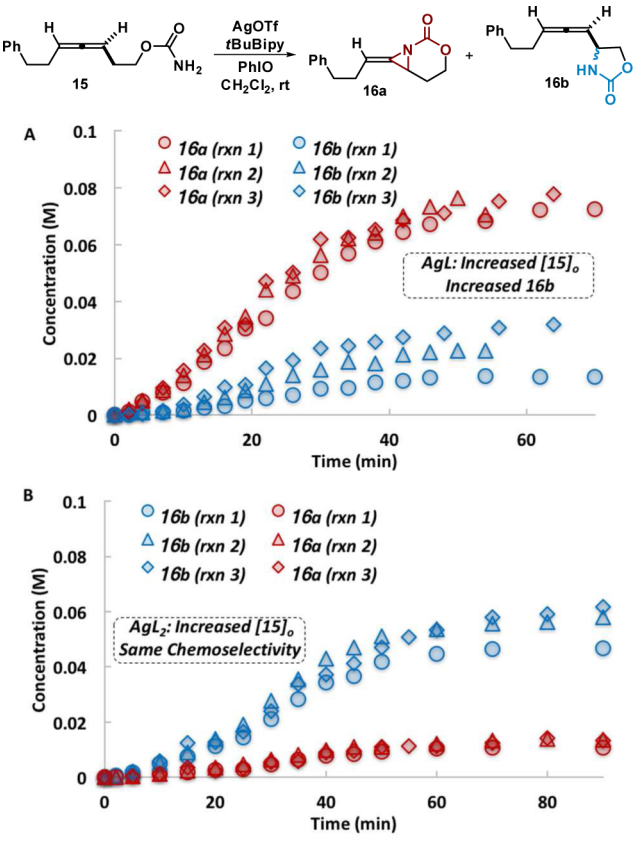

Figure 6. Reaction profiles showing product formation: (A) AgOTf:ligand = 1:1.25; (B) AgOTf:ligand = 1:3. Conditions: reaction 1, $[15]_0$ = 0.08 M; reaction 2, $[15]_0$ = 0.10 M; reaction 3, $[15]_0$ = 0.12 M.

DOI: 10.1021/acs.organomet.7b00190
Organometallics XXXX, XXX, XXX−XXX

amination when a 1:3 Ag:ligand ratio was used (Figure 6B). The sensitivity of the C−H amination rate to initial carbamate **15** concentration (with the AgL-type system) is likely due to a small perturbation in the population of catalyst among AgL, AgL_2, and $(Ag_xL_y)_n$ oligomeric states. Due to the insolubility of the PhIO, it is unlikely that the steady-state concentration of imidoiodinane is affected by the initial concentration of **15**. Instead, it is possible that the carbamate itself may coordinate to the metal center, shifting the catalyst equilibria toward the AgL_2-type species, leading to a shift in the relative concentration of key intermediates ***Int-1*** and ***Int-2***, assuming the rates of combination between imidoiodinane and either AgL or AgL_2 are similar (Figure 5). Thus, the chemoselectivity and overall rate of reaction are primarily controlled by the partitioning of the catalytic species among AgL, AgL_2, and $(Ag_xL_y)_n$ oligomer.

We next investigated how allylic deuteration of the substrate affects both the rate of the carbamate **15** consumption and the chemoselectivity. Previous studies with **30-D** (Scheme 8A)

Scheme 8. Intrinsic Kinetic Isotope Effects

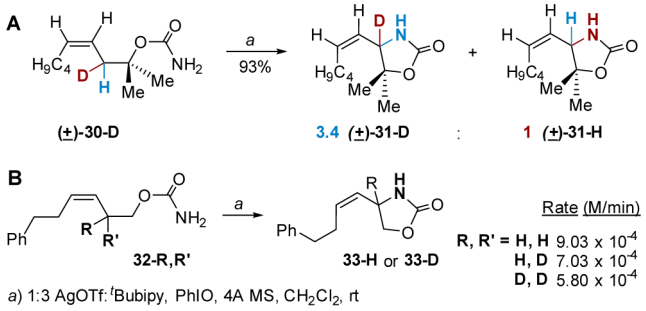

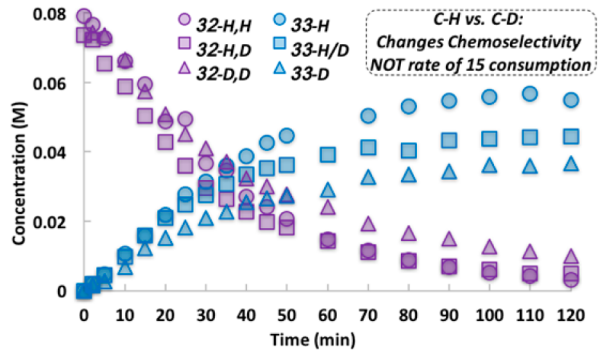

showed an intrinsic primary kinetic isotope effect (KIE) of 3.4, which is lower than the KIEs of 4−12 typically observed for stepwise C−H amination processes.[15d] This value is closer to the intrinsic KIE of 1.9 previously observed for $Rh_2(OAc)_4$ and also compares well to the KIEs of 2.9 and 2.6 obtained for nitrene transfer reactions promoted by $Rh_2(esp)_2$ and $Rh_2(espn)_2$, respectively.[15j,18b] However, relating intrinsic initial rate only to the product distribution (**31-D** vs **31-H**) neglects possible changes in chemoselectivity in favor of aziridination resulting from isotope incorporation. To address this issue, the reaction profile for C−H aminations involving protiated, monodeuterated, and dideuterated versions of the homoallylic carbamate **32** were measured (Scheme 8B).

The rates of consumption of carbamate **32** were nearly identical, irrespective of the isotope incorporation pattern. This is expected, since regardless of isotopic composition, either dissolution of the PhIO or the reaction of the carbamate with PhIO to form the imidoiodinane is rate-limiting. However, the rates of C−H insertion to yield **33** progressively decreased upon increasing the extent of allylic deuteration. The discrepancy in the mass balance is compensated for by a concomitant increase in the relative amount of the aziridination product (not shown). This experiment reveals that the chemoselectivity, but not the overall rate of conversion, is sensitive to allylic deuteration, suggesting that C−H bond cleavage is irreversible and represents the selectivity-determining step to yield the C−H aminated product. However, it should be noted that the C−H bond cleavage is not a crucial rate-controlling step in the context of the overall catalytic network. By strengthening the key allylic bond (through C−H/C−D incorporation), the product can be diverted toward the aziridination pathway without significantly affecting the overall rate of consumption of the carbamate starting material **15**. This result also reveals that the C−H amination and aziridination pathways are connected via a series of intermediates related by dynamic equilibria; thus, C−N bond formation likely represents the first irreversible step in the respective pathways of the parallel catalytic cycles, with k_1 being the rate-limiting step.

The proposed mechanism for both reaction pathways is illustrated in Scheme 9. PhIO oxidizes the carbamate **15** to form an intermediate imidoiodinane species, **34**. The reversibility of this process, most likely by reaction with adventitious water, competes with productive reaction of the imidoiodinane with the Ag catalyst to form the active metal nitrene species, **35** and **36**, respectively, through ***Int-1*** and ***Int-2***. The interplay between condensation and hydrolysis by adventitious water is supported by the fact that incorporation of molecular sieves into the reaction is key to the success of both aziridination and amination reactions. The heterogeneous nature of the oxidant also plays a crucial role by limiting the concentration of the highly reactive, unbound nitrene intermediates. This feature may allow the silver catalyst to turn over the oxidized material **34** as it is being generated, preventing undesirable side reactions that include dimerization of the nitrene precursor or decomposition of the product. This hypothesis is supported by the observation that common soluble hypervalent iodine oxidants, including the $PhI(OAc)_2$, $PhI(OMe)_2$, or $PhI(OPiv)_2$ oxidants, that work well with Rh catalysts and sulfamate-based nitrene precursors show either poor chemoselectivity or no significant reactivity with carbamates in the presence of molecular sieves or MgO as additives. This observation may be attributed to two factors. First, when zero to poor conversion is observed, the soluble hypervalent iodine reagent may not be oxidizing enough to transform the carbamate to the intermediate imidoiodinane. Since sulfamates are easier to oxidize in comparison to the corresponding carbamates, they give good conversion to products but provide no tunable chemoselectivity. A second factor may be competing coordination of the released carboxylate to the Ag center when employing soluble oxidants, despite efforts to use additives (molecular sieves, MgO) to sequester these species.

The ability of PhIO to promote highly chemoselective Ag-catalyzed nitrene transfer is a unique feature of silver chemistry that stands in contrast to other metal-catalyzed nitrene transfer reactions.[3−10] Though neither the PhIO oxidant nor the required molecular sieves are soluble in CH_2Cl_2, kinetic profiles were highly reproducible for individual batches of substrate. All kinetic profiles that are explicitly compared were obtained using

DOI: 10.1021/acs.organomet.7b00190
Organometallics XXXX, XXX, XXX−XXX

Scheme 9. Proposed Mechanisms of Chemodivergent Aziridination and C−H Amination

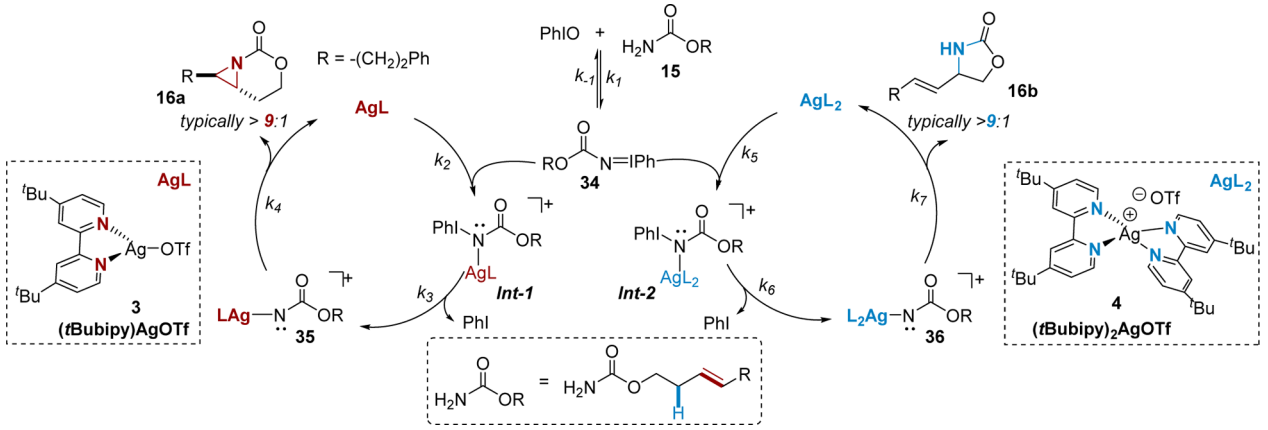

a single batch of substrate and PhIO. An excess of PhIO was typically employed to ensure that the reaction would proceed to completion, although 2 equiv could be used with success. The better reproducibility of our results using an excess of PhIO was attributed to slow decomposition of the oxidant during the reaction or potential interactions with the carbamate product that might tie up some available oxidant.

Once they are generated, the silver nitrene intermediates **35** and **36** carry out either stepwise aziridination to **16a** or C−H insertion to **16b**, respectively, followed by barrierless radical recombination, depending on the coordination number at the metal center. It is likely that the coordination environment at the metal influences the trajectory of approach of the substrate to the metal. A low-coordinate Ag may engage the alkene in binding, promoting aziridination, while a higher-coordinate Ag may disfavor such an interaction, leading to favored C−H insertion. Calculations carried out by the Pérez group on Ag complexes supported by trispyrazolylborate (Tp) ligands indicate that the aziridination pathway proceeds by attack of a triplet nitrene species on the alkene to form the first C−N bond.[15h] The triplet then crosses over to the singlet state and products form before any true intermediates are reached; the resulting reaction pathway thus appears concerted in nature, albeit asynchronous. We have reported an analogous mechanism for C−H amination by silver nitrene species,[25] involving an HAT transition state on the triplet potential energy surface followed by intersystem crossing to the singlet state and subsequent product formation with no intermediates encountered. Our studies of the C−H insertion pathway here also imply a mechanism in which no intermediates are encountered, with the C−H cleavage event functioning as the selectivity-determining step for that particular cycle.

Taken together, this suite of classical physical organic and kinetic experiments distinguishes our system from other chemoselective nitrene transfer catalyst systems in two important ways. First, experiments support single-step mechanisms for both the C−H amination and aziridination pathways. In other catalyst systems selective for C−H amination, high chemoselectivity for allylic C−H amination is attributed to the metal nitrene's high propensity for H atom abstraction in a stepwise mechanism that essentially passes through an HAT transition state.[9,10,12] Second, Ag catalysis displays a complex dependence on both the stability and population of the reactive intermediates. While the overall reaction rate is primarily controlled by imidoiodinane formation, as seen in DuBois's Rh-based systems, chemoselectivity is a consequence of both the relative speciation of the silver center and the differences in the rate constants for the key oxidative step (k_3 for aziridination and k_6 for amination; Scheme 8) for each parallel cycle. The behavior of the system using varied ligand loadings and varied initial substrate concentrations suggests that the aziridination pathway is intrinsically faster than the C−H amination reaction. However, the combination of low imidoiodinane concentration, due to low solubility of the PhIO oxidant, and the ability to partition the silver between multiple coordination environments accounts for the observed behavior.

CONCLUSIONS

In conclusion, the experimental studies described herein provide insight into both silver catalyst structure and its effect on tunable, chemoselective nitrene transfer reactions. Spectroscopic studies indicate that the two distinct silver catalysts differ in coordination number but not in nuclearity; both species are monomeric in the resting state. Mechanistic and computational studies support the formation of electronically similar putative silver nitrenes from both AgLOTf and AgL_2OTf. Both the aziridination and C−H bond amination reaction pathways display similar mechanisms and kinetic behavior; thus, the primary feature governing chemoselectivity involves steric differences in the catalysts.

The kinetic analysis obtained from these experiments has significant implications for understanding the chemoselectivity of dynamic Ag-catalyzed aziridination and C−H amination via nitrene transfer. The two paths show a similar dependence on substrate and catalyst concentration, as well as similar overall maximum rates for consumption of **15**. The two reaction pathways likely do not differ in terms of early kinetically significant mechanistic steps, regardless of the catalyst identity. The inclusion of kinetic profiling to examine the behavior of both catalytic pathways provided information concerning reaction behavior that cannot be obtained with traditional initial rate studies. Exploring the full course of the reaction indicates that steady-state kinetics are, in fact, very similar for both the AgLOTf and AgL_2OTf species and that the steric environment surrounding the putative nitrene influences the chemoselectivity of the reaction. The insights from this work have implications in our ongoing development of new ligands with variable steric properties to enable catalyst-controlled, site-selective C−H aminations in the presence of multiple potential reactive C−H bonds.

DOI: 10.1021/acs.organomet.7b00190
Organometallics XXXX, XXX, XXX−XXX

EXPERIMENTAL SECTION

General Methods. All glassware was oven-dried overnight at 130 °C or flame-dried under a stream of dry nitrogen prior to use. Unless otherwise specified, reagents were used as obtained from the vendor without further purification. Tetrahydrofuran and diethyl ether were freshly distilled from purple Na/benzophenone ketyl. Dichloromethane was dried over CaH_2 and freshly distilled prior to use. Air- and moisture-sensitive reactions were performed using standard Schlenk techniques under an atmosphere of nitrogen. Analytical thin-layer chromatography (TLC) was performed utilizing precoated silica gel 60 F_{254} plates containing a fluorescent indicator, while preparative chromatography was performed using SilicaFlash P60 silica gel (230−400 mesh). Unless otherwise stated, the mobile phases for column chromatography were hexanes/ethyl acetate mixtures, using a gradient method, beginning with 100% hexanes and gradually increasing the polarity using ethyl acetate. Stains used to visualize reaction products included *p*-anisaldehyde, $KMnO_4$, ceric ammonium molybdate (CAM stain), and iodine powder. ^{1}H NMR and ^{13}C NMR spectra were obtained using Bruker 400 and Bruker Callisto-500 spectrometers. For ^{1}H NMR, chemical shifts are reported relative to residual protiated solvent peaks (δ 7.26, 2.49, 7.15, and 7.09 ppm for $CDCl_3$, $(CD_3)_2SO$, C_6D_6, and $CD_3C_6D_5$, respectively). ^{13}C NMR spectra were measured at 125, 100, or 75 MHz on the same instruments noted above for recording ^{1}H NMR spectra. All *J* values represent $^3J_{H-H}$ coupling values unless otherwise indicated. The ^{1}H spectra were not decoupled, while the ^{13}C NMR spectra were ^{1}H-decoupled. Chemical shifts were again reported in accordance with residual protiated solvent peaks (δ 77.2, 39.5, 128.0, and 137.9 ppm for $CDCl_3$, $(CD_3)_2SO$, C_6D_6, and $CD_3C_6D_5$, respectively). Accurate mass measurements were acquired at the University of Wisconsin, Madison, WI, using a Micromass LCT instrument (electrospray ionization, time-of-flight analyzer, or electron impact method).

Synthesis of Carbamates. Carbamate substrates were synthesized using the same general procedure. The corresponding alcohol (between 0.5 and 3.0 g, 1 equiv) was dissolved in dichloromethane (0.3 M) and placed in an ice bath at 0 °C. Freshly distilled trichloroacetyl isocyanate (1.2 equiv) was added dropwise over 30 s to 1 min. The ice bath was removed and the reaction mixture stirred until TLC indicated complete consumption of the starting material (0.75−2 h). The solvent was removed and the crude reaction mixture dissolved in methanol (0.2 M). Potassium carbonate (0.2 equiv) was added and the reaction mixture stirred at room temperature until TLC indicated completion, usually 4−8 h. Saturated aqueous NH_4Cl was added and the mixture extracted with three portions of dichloromethane. The combined organic phases were washed with brine, dried with sodium sulfate, filtered, and concentrated under reduced pressure. The crude products were purified by silica gel column chromatography. Depending on the purity of the trichloroacetyl isocyanate, traces of trichloroacetamide were detected in the carbamate by ^{13}C NMR, even after chromatographic purification. This impurity was found to significantly alter the rate and chemoselectivity of the reaction. To remove the trichloroacetamide, the carbamate was dissolved in CH_2Cl_2 to form a 0.1 M solution. An equal volume of 1.0 M NaOH was added, and the reaction mixture was stirred vigorously for 5 min. The layers were separated, and the aqueous layer was extracted three times with an equal volume of CH_2Cl_2. The organic layers were combined, dried with sodium sulfate, filtered with cotton, and concentrated under reduced pressure.

Compound ***17***. The product was obtained in 81% yield from 287 mg (1.20 mmol) of the corresponding alcohol. ^{1}H NMR (500 MHz, $CDCl_3$): δ 7.38−7.25 (m, 4H), 7.25−7.15 (m, 5H), 7.15−7.07 (tt, *J* = 7.0, 1.6 Hz (^4J), 1H), 4.69 (s, 2H), 4.15 (dt, *J* = 10.6, 6.6 Hz, 1H), 4.10 (dt, *J* = 10.6, 6.6 Hz, 1H), 1.80 (dtd, *J* = 13.9, 6.8, 5.3 Hz, 1H), 1.73−1.64 (m, 1H), 1.33−1.18 (overlapping multiplets, 2H), 1.12−0.95 (ddt, J = 14.1, 8.7, 6.5 Hz, 1H). ^{13}C NMR (126 MHz, $CDCl_3$): δ 157.2, 147.1, 141.6, 130.7, 128.5, 128.4, 128.0, 126.6, 126.0, 65.1, 35.3, 30.6, 22.8, 20.4. HRMS (ESI): *m/z* calculated for $C_{18}H_{19}NO_2$ [M + H^+], 282.1489; found, 282.1484.

Compound ***20a***. The product was obtained in 84% yield from 127 mg (0.524 mmol) of the corresponding alcohol. ^{1}H NMR (500 MHz, $CDCl_3$): δ 7.28 (dd, *J* = 8.0, 6.6 Hz, 2H), 7.23−7.18 (m, 3H), 7.11 (d, *J* = 8.6 Hz, 2H), 6.83 (d, *J* = 8.6 Hz, 2H), 5.15 (p, *J* = 6.4 Hz, 1H), 4.51 (br s, 2H), 3.79 (s, 3H), 2.85 (d, *J* = 6.4, 2.9 Hz (^4J), 2H), 2.80 (dd, *J* = 6.4, 2.9 Hz (^4J), 2H). ^{13}C NMR (126 MHz, $CDCl_3$): δ 158.4, 156.5, 137.8, 130.7, 129.7, 128.5, 126.6, 114.0, 76.3, 55.4, 40.0, 39.2. HRMS (ESI): *m/z* calculated for $C_{17}H_{19}NO_3$ [M + NH_4^+], 303.1704; found, 303.1707.

Compound ***20b***. The product was obtained in 94% yield from 159 mg (0.702 mmol) of the corresponding alcohol. ^{1}H NMR (500 MHz, $CDCl_3$): δ 7.28 (dd, *J* = 8.0, 6.6 Hz, 2H), 7.24−7.17 (m, 3H), 7.08 (apparent s, 4H), 5.18 (p, *J* = 6.4 Hz, 1H), 4.49 (s, 2H), 2.88−2.79 (overlapping second-order multiplets, 4H), 2.32 (s, 3H). ^{13}C NMR (126 MHz, $CDCl_3$): δ 156.5, 137.8, 136.2, 134.5, 129.7, 129.6, 129.3, 128.5, 126.6, 76.2, 40.0, 39.7, 21.3. HRMS (ESI): *m/z* calculated for $C_{17}H_{19}NO_2$ [M + NH_4^+], 287.1755, found, 287.1749.

Compound ***20c***. The product was obtained in 92% yield from 190 mg (0.797 mmol) of the corresponding alcohol. ^{1}H NMR (500 MHz, $CDCl_3$): δ 7.31−7.26 (m, 2H), 7.24−7.17 (m, 4H), 6.81−6.72 (m, 3H), 5.19 (p, *J* = 6.5 Hz, 1H), 4.57 (s, 2H), 3.78 (s, 3H), 2.91−2.79 (overlapping m, 4H). ^{13}C NMR (126 MHz, $CDCl_3$): δ 159.7, 156.5, 139.3, 137.7, 129.7, 129.5, 128.5, 126.7, 122.1, 115.4, 112.0, 55.4, 40.1. HRMS (ESI): *m/z* calculated for $C_{17}H_{19}NO_3$ [M + H^+], 286.1438; found, 286.1444.

Compound ***20d***. The product was obtained in 87% yield from 434 mg (1.49 mmol) of the corresponding alcohol. ^{1}H NMR (500 MHz, $CDCl_3$): δ 7.39 (d, *J* = 8.3 Hz, 2H), 7.28 (dd, *J* = 8.1, 6.6 Hz, 2H), 7.25−7.21 (m, 1H), 7.20−7.15 (m, 2H), 7.05 (d, *J* = 8.3 Hz, 2H), 5.14 (p, *J* = 6.4 Hz, 1H), 4.69 (s, 2H), 2.81 (dd, *J* = 14.0, 6.4, 1H), 2.74 (dd *J* = 14.0, 6.4) 2.71−2.69 (overlapping multiplets, 2H). ^{13}C NMR (126 MHz, $CDCl_3$): δ 156.5, 137.4, 136.7, 131.6, 131.4, 129.6, 128.6, 126.8, 120.6, 75.7, 40.2, 39.4. HRMS (ESI): *m/z* calculated for $C_{16}H_{16}BrNO_2$ [M + NH_4^+], 351.0698; found, 351.0703.

Compound ***20e***. The product was obtained in 94% yield from 229 mg (0.797 mmol) of the corresponding alcohol. ^{1}H NMR (500 MHz, $CDCl_3$): δ 7.53 (d, *J* = 8.0 Hz, 2H), 7.32−7.27 (m, 4H), 7.25−7.21 (m, 1H), 7.21−7.17 (d, *J* = 8.0 Hz, 2H), 5.20 (p, *J* = 6.5 Hz, 1H), 4.66 (s, 2H), 2.96−2.87 (overlapping multiplets, 3H), 2.84 (dd, *J* = 13.9, 6.5 Hz, 1H). ^{13}C NMR (126 MHz, $CDCl_3$): δ 159.7, 156.5, 139.3, 137.7, 129.7, 129.5, 128.5, 126.7, 122.1, 115.4, 112.0, 55.4, 40.1. HRMS (ESI): *m/z* calculated for $C_{17}H_{16}F_3NO_2$ [M + NH_4^+], 341.1472; found, 341.1474.

Compound ***32****-H,H*. The product was purified by column chromatography using a 0 → 50% gradient of ethyl acetate in hexanes with 10% increments. The resulting white solid was isolated in 90% yield. ^{1}H NMR (500 MHz, $CDCl_3$): δ 7.30−7.26 (m, 2H), 7.21−7.15 (m, 3H), 5.58−5.51 (m, 1H), 5.41−5.34 (m, 1H), 4.53 (broad s, 2H), 3.99 (t, *J* = 6.8 Hz, 2H), 2.67 (dd, *J* = 8.5, 6.9 Hz, 2H), 2.41−2.35 (m, 2H), 2.32 (qd, *J* = 7.0, 1.5 Hz (^4J), 2H). ^{13}C NMR (126 MHz, $CDCl_3$): δ 156.9, 142.0, 131.8, 128.6, 128.4, 126.0, 125.4, 64.7, 36.0, 29.4, 27.3. HRMS (ESI): *m/z* calculated for $C_{13}H_{18}NO_2$ [M + $H]^+$, 220.1332; found, 220.1331.

Compound ***32****-H,D*. Synthesized according to the general procedure above. The product was purified by column chromatography using a 0 → 50% gradient of ethyl acetate in hexanes with 10% increments. The resulting white solid was obtained in 90% yield. ^{1}H NMR (500 MHz, $CDCl_3$): δ 7.31−7.26 (m, 2H), 7.21−7.16 (m, 3H), 5.55 (dtd, *J* = 11.0, 7.3, 1.5 (^4J) Hz, 1H), 5.40−5.34 (m, 1H), 4.55 (s, 2H), 3.98 (d, *J* = 6.8 Hz, 2H), 2.67 (dd, *J* = 8.5, 6.9 Hz, 2H), 2.38 (qd, *J* = 7.5, 1.5 (^4J) Hz, 2H), 2.36−2.25 (m, 1H). ^{13}C NMR (126 MHz, $CDCl_3$): δ 156.9, 142.0, 131.8, 128.6, 128.4, 126.0, 125.4, 64.6, 36.0, 29.4, 26.9 (1:1:1 t, *J* = 19.5 Hz). HRMS (ESI): *m/z* calculated for $C_{13}H_{17}DNO_2$ [M + $H]^+$, 221.1395; found, 221.1394.

Compound ***32****-D,D*. The product was purified by column chromatography using a 0 → 50% gradient of ethyl acetate in hexanes with 10% increments. The resulting white solid was isolated in 74% yield with 91% D incorporation. ^{1}H NMR (500 MHz, $CDCl_3$): δ 7.31−7.26 (m, 2H), 7.21−7.16 (m, 3H), 5.55 (dt, *J* = 10.9, 7.3 Hz, 1H), 5.37 (d, *J* = 10.8 Hz, 1H), 4.54 (s, 2H), 3.98 (s, 2H), 2.67 (dd, *J*

DOI: 10.1021/acs.organomet.7b00190
Organometallics XXXX, XXX, XXX−XXX

= 8.5, 6.9 Hz, 2H), 2.38 (qd, J = 7.6, 1.5 Hz (^4J), 2H). ^{13}C NMR (126 MHz, $CDCl_3$): δ 156.8, 141.8, 131.7, 128.5, 128.3, 125.9, 125.1, 64.4, 35.8, 29.2, 26.9−26.1 (m). HRMS (ESI): m/z calculated for $C_{13}H_{16}D_2NO_2$ $[M + H]^+$, 221.1458; found, 221.1457.

General Amination Procedure. A predried reaction flask was charged with AgOTf (0.10 equiv), ligand (0.125 or 0.3 equiv), and powdered 4 Å molecular sieves (4 times the substrate mass). CH_2Cl_2 (0.02 M in AgOTf) was added, and the mixture was stirred vigorously for 15 min. A solution of the carbamate (1 equiv) in CH_2Cl_2 (0.2 M in substrate) was placed in the reaction flask. After 2 min, PhIO (3.5 equiv) was added in one portion and the reaction mixture was stirred at room temperature until TLC indicated complete consumption of the starting material (2−14 h). The reaction mixture was filtered through a glass frit and the filtrate concentrated under reduced pressure. The crude products were purified by silica gel column chromatography using a hexane/EtOAc gradient.

In the cases of radical inhibition experiments, 10 mol % of a radical inhibitor was added at the outset of the reaction.

Compound ***18***. When 0.30 equiv of 4,4′-di-*tert*-butylbipyridine was used as the ligand with 56 mg (0.20 mmol) of the corresponding carbamate, the product was obtained in 3:1 dr in 48% yield after 6.5 h. The remaining mass balance was unreacted starting material. The relative stereochemistry of the products was not determined. Major diastereomer: ^{1}H NMR (500 MHz, $CDCl_3$) δ 7.36−7.22 (m, 9H), 7.22−7.17 (m, 1H), 5.14 (s, 1H), 4.44 (t, J = 8.5 Hz, 1H), 4.27 (dd, J = 8.5, 6.4 Hz, 1H), 3.01 (dddd, J = 9.7, 8.5, 6.4, 1.2 Hz (^4J), 1H), 1.97 (ddd, J = 9.7, 8.8, 5.4 Hz, 1H), 1.44 (t, J = 5.4 Hz, 1H), 1.31−1.19 (m, 1H); ^{13}C NMR (126 MHz, $CDCl_3$) δ 159.1, 144.8, 140.4, 129.3, 129.2, 128.6, 128.3, 127.27, 126.7, 70.1, 54.2, 35.6, 29.4, 16.2; HRMS (ESI) m/z calculated for $C_{18}H_{17}NO_2$ $[M + NH_4^+]$ 297.1598, found 297.1591. Minor diastereomer: ^{1}H NMR (500 MHz, $CDCl_3$) δ 7.35−7.31 (m, 2H), 7.30−7.23 (m, 5H), 7.22−7.11 (m, 3H), 4.53 (s, 1H), 4.42 (t, J = 8.4 Hz, 1H), 4.36 (dd, J = 8.4, 6.2 Hz, 1H), 3.31 (td, J = 8.4, 6.2 Hz, 1H), 1.92 (td, J = 8.4, 5.7 Hz, 1H), 1.35 (dd, J = 8.6, 5.7 Hz, 1H), 1.28−1.25 (m, 1H); ^{13}C NMR (126 MHz, $CDCl_3$) δ 158.8, 145.2, 140.6, 130.0, 129.3, 128.8, 127.8, 127.6, 126.7, 70.6, 54.1, 35.4, 31.2, 17.8; HRMS (ESI) m/z calculated for $C_{18}H_{17}NO_2$ $[M + NH_4^+]$ 297.1598, found 297.1593.

Compound ***29-H***. The product was purified by column chromatography using a 0 → 50% gradient of ethyl acetate in hexanes with 10% increments. The resulting white solid was isolated in 58% yield. ^{1}H NMR (500 MHz, $CDCl_3$): δ 7.34−7.29 (m, 2H), 7.26−7.22 (m, 1H), 7.16−7.12 (m, 2H), 5.70−5.61 (m, 1H), 5.35 (ddt, J = 10.7, 9.5, 1.3 Hz (^4J), 1H), 4.31 (dddd, J = 9.4, 8.3, 7.2, 1.0 Hz (^4J), 1H), 4.12 (t, J = 8.5 Hz, 1H), 4.12 (overlapping broad s, 1H), 3.72 (dd, J = 8.6, 7.1 Hz, 1H), 2.75 (ddd, J = 13.2, 7.2, 5.8 Hz, 1H), 2.65 (ddd, J = 13.7, 8.3, 5.9 Hz, 1H), 2.47−2.32 (m, 2H). ^{13}C NMR (126 MHz, $CDCl_3$): δ 159.1, 141.0, 133.8, 129.1, 128.6, 128.6, 126.6, 69.9, 49.4, 35.3, 29.7. HRMS (ESI): m/z calculated for $C_{13}H_{16}NO_2$ $[M + H]^+$, 218.1176, found 218.1175.

Compound ***29-D***. The product was purified by column chromatography using a 0 → 50% gradient of ethyl acetate in hexanes with 10% increments. The resulting clear oil was isolated in 26% yield. ^{1}H NMR (500 MHz, $CDCl_3$): δ 7.34−7.27 (m, 2H), 7.25−7.21 (m, 1H), 7.16−7.10 (m, 2H), 5.65 (dt, J = 10.8, 8.0 Hz, 1H), 5.34 (d, J = 10.7 Hz, 1H), 4.75 (s, 1H), 4.09 (d, J = 8.6 Hz, 1H), 3.69 (d, J = 8.6 Hz, 1H), 2.75−2.62 (m, 2H), 2.47−2.30 (m, 2H). ^{13}C NMR (126 MHz, $CDCl_3$): δ 159.4, 141.0, 133.7, 129.0, 128.5, 128.5, 126.5, 69.8, 49.1 (1:1:1 t, J = 22.1 Hz), 35.3, 29.7. HRMS (ESI): m/z calculated for $C_{13}H_{15}DNO_2$ $[M + H]^+$, 219.1238, found 219.1238.

General Procedure for Acquisition of Kinetic Data. A predried 10 mL round-bottom flask was charged with AgOTf (0.04−0.20 equiv), ligand (1.25 or 3 equiv relative to AgOTf), phenanthrene (approximately 0.06 M in CH_2Cl_2), and powdered 4 Å molecular sieves (1 g/mmol of substrate). CH_2Cl_2 was added, and the mixture was stirred vigorously for 15 min. A solution of the carbamate (1 equiv) in CH_2Cl_2 (0.025−0.4 M in substrate) was added to the reaction flask. After 2 min, PhIO was added in one portion, marking t = 0, and the reaction mixture was stirred at room temperature. Aliquots (20 μL) were removed at regular intervals by autopipet and injected into 1.5 mL mixtures of HPLC grade 10/90 iPrOH/hexanes. The mixtures were filtered and analyzed with a Shimadzu HPLC instrument, Model LC-20AB, equipped with a YMC silica column, PV12505-2506WT, with dimensions 250 × 6.0 mm. The column was eluted with a 10/90 iPrOH/hexanes mobile phase and monitored at 210 nm, Concentrations of major reaction components were determined according to the calibration curves illustrated in Figures S3−S6 in the Supporting Information. Validation of HPLC−UV−vis as a method of analysis was performed by concentration of HPLC samples attained using the above method. The samples were concentrated, dissolved in approximately 1 mL of $CDCl_3$, and analyzed by ^{1}H NMR with a 10 s receiver delay. Reasonable agreement between these two methods of analysis confirms HPLC−UV−vis as a valid method for monitoring these reactions.

Measuring Initial Rates by NMR Kinetics for 26 and 28. A predried reaction 10 mL round-bottom flask was charged with AgOTf (0.10 equiv), ligand (0.125 or 0.3 equiv), mesitylene (10 μL, 0.0719 mmol), and powdered 4 Å molecular sieves (1 g/mmol of substrate). CH_2Cl_2 (1.25 mL) was added, and the mixture was stirred vigorously for 15 min. A solution of the carbamate (0.25 mmol, 1 equiv) in CH_2Cl_2 (1.25 mL, overall 0.1 M in substrate) was placed in the reaction flask. After 2 min, PhIO (2 equiv or 3.5 equiv) was added in one portion, marking t = 0, and the reaction mixture was stirred at room temperature. Aliquots were removed every 3 min and analyzed by NMR.

Computational Methods. The crystal structure geometries VIJZOE[36] and ESERUQ[37] were used as starting points for geometry optimization of $[Ag(bpy)_2]^+$ and Ag(bpy)(OTf) species, respectively. The Avogadro program[38] was used to build a clean model of the nitrogen substrate and to add this substrate to the starting silver complexes (Figure S28 in the Supporting Information). Restricted Kohn−Sham geometry optimizations were performed on the ORCA electronic structure package[39] using the GGA functional BP86[40,41] with the Ahlrichs TZV basis set[42,43] including polarization functions from the TurboMole library.[44] All calculations utilized the scalar relativistic zeroth-order regular approximation (ZORA) and the COSMO solvent model for CH_2Cl_2.[45] Transition states were identified as such by the observation of a single vibrational mode with a negative frequency. The motions involved with these modes were confirmed (by inspection) to coincide with the reaction coordinate.

Optimized structures are based on a silver complex containing either one *t*Bubipy ligand and one OTf ligand or two *t*Bubipy ligands: i.e., starting from Ag(*t*Bubipy)(OTf) (**3**) or $[Ag(tBubipy)_2]^+$ (**4**). Imidoiodinane adducts of **3** and **4** were optimized using imidoiodinane **23** to give Ag(*t*Bubipy)(OTf)(imidoiodinane) (**24a**) and $[Ag(tBubipy)_2$(imidoiodinane)$]^+$ (**25a**), respectively. Dissociation of PhI from **24a** or **25a** to yield the nitrene complexes Ag(*t*Bubipy)(OTf)(nitrene) (**24b**) and $[Ag(tBubipy)_2$(nitrene)$]^+$ (**25b**) was examined using a relaxed surface scan that elongated the N−I bond distance from the normal bond distance of ∼2.1 Å to a nonbonding distance of ∼5 Å. The transformation **24a** → **24b** + PhI has ΔG = +57 kJ/mol, while **25a** → **25b** + PhI with ΔG = +36 kJ/mol is more facile, as expected on the basis of the difference in sterics. Neither of these two processes passes through a transition state.

The geometry of each maximum was used for a transition state search, and the energies of these transition states (**24b**(TSaz) for the aziridination transition state and **24b**(TSCH) for the C−H amination transition state) and reaction products (**24b**(Paz) for the aziridination product and **24b**(PCH) for the C−H amination product) are given in Table S7 in the Supporting Information. Geometries for each species are shown in Figures S36−S55 in the Supporting Information, and sketches of the potential energy surfaces are given in Figures S30, S31, and S33 in the Supporting Information.

■ ASSOCIATED CONTENT

Supporting Information

The Supporting Information is available free of charge on the ACS Publications website at DOI: 10.1021/acs.organomet.7b00190.

DOI: 10.1021/acs.organomet.7b00190
Organometallics XXXX, XXX, XXX−XXX

Experimental procedures and characterization data for known compounds and intermediates, calibration curves, kinetic plots, and computational details (PDF)
Cartesian coordinates of the calculated structures (XYZ)

AUTHOR INFORMATION

Corresponding Authors

*E-mail for J.F.B.: berry@chem.wisc.edu.
*E-mail for J.E.H.: jhein@chem.ubc.ca.
*E-mail for J.M.S.: schomakerj@chem.wisc.edu.

ORCID

Jason E. Hein: 0000-0002-4345-3005
Jennifer M. Schomaker: 0000-0003-1329-950X

Present Address

[§]Department of Chemistry, University of Pennsylvania, Philadelphia, PA 19104-6323, USA.

Notes

The authors declare no competing financial interest.

ACKNOWLEDGMENTS

This work was funded through the Wisconsin Alumni Research Foundation to J.M.S. J.F.B. thanks the Center for Selective C−H Functionalization supported by the National Science Foundation (CHE01205646). J.E.H. thanks the Natural Sciences and Engineering Research Council of Canada (RGPIN-2016-04613) for support via the Discovery Grants program. The authors thank Professor Robert Bergman for helpful advice and comments on this manuscript.

REFERENCES

(1) For selected references on selective C−H functionalizations, see: (a) Lescot, C.; Darses, B.; Collet, F.; Retailleau, P.; Dauban, P. *J. Org. Chem.* **2012**, *77*, 7232−7240. (b) Newhouse, T.; Baran, P. S. *Angew. Chem., Int. Ed.* **2011**, *50*, 3362−3374. (c) Bess, E. N.; DeLuca, R. J.; Tindall, D. J.; Oderinde, M. S.; Roizen, J. L.; Du Bois, J.; Sigman, M. S. *J. Am. Chem. Soc.* **2014**, *136*, 5783−5789. (d) Chen, M. S.; White, M. C. *Science* **2007**, *318*, 783−7. (e) Chen, M. S.; White, M. C. *Science* **2010**, *327*, 566−71. (f) White, M. C. *Science* **2012**, *335*, 807−809. (g) Bagchi, V.; Paraskevopoulou, P.; Das, P.; Chi, L.; Wang, Q.; Choudhury, A.; Mathieson, J. S.; Cronin, L.; Pardue, D. B.; Cundari, T. R.; Mitrikas, G.; Sanakis, Y.; Stavropoulos, P. *J. Am. Chem. Soc.* **2014**, *136*, 11362−11381. (h) Gormisky, P.; White, M. C. *J. Am. Chem. Soc.* **2013**, *135*, 14052−5. (i) Sharma, A.; Hartwig, J. H. *Nature* **2015**, *517*, 600−604. (j) McNally, A.; Haffemeyer, B.; Collins, B. S. L.; Gaunt, M. J. *Nature* **2014**, *510*, 129−133. (k) Kornecki, K. P.; Berry, J. F.; Powers, D. C.; Ritter, T. *Prog. Inorg. Chem.* **2014**, *58*, 225−302.

(2) For general references on the synthesis and importance of amines, see: (a) Lawrence, S. A. *Amines: Synthesis, Properties and Applications*; Cambridge University Press: New York, NY, 2004. (b) Nugent, T. C.; El-Shazly, M. *Adv. Synth. Catal.* **2010**, *352*, 753−819. (c) Smith, M. B. In *Compendium of Organic Synthetic Methods*; Wiley: New York, NY, 2009; Vol. *12*. (d) Emerson, W. S. The Preparation of Amines by Reductive Alkylation. In *Organic Reactions*; Wiley: New York, NY, 2004. (e) Afagh, N. A.; Yudin, A. K. *Angew. Chem., Int. Ed.* **2010**, *49*, 262−310.

(3) For selected examples of reviews on nitrene transfers, see: (a) Zalatan, D. N.; Du Bois, J. *Top. Curr. Chem.* **2009**, *292*, 347−378. (b) Muller, P.; Fruit, C. *Chem. Rev.* **2003**, *103*, 2905−20. (c) Li, Z. G.; He, C. *Eur. J. Org. Chem.* **2006**, *2006*, 4313−4322. (d) Halfen, J. A. *Curr. Org. Chem.* **2005**, *9*, 657−69. (e) Dequirez, G.; Pons, V.; Dauban, P. *Angew. Chem., Int. Ed.* **2012**, *51*, 7384−95. (f) Collet, F.; Dodd, R. H.; Dauban, P. *Chem. Commun.* **2009**, *34*, 5061−74. (g) Collet, F.; Lescot, C.; Dauban, P. *Chem. Soc. Rev.* **2011**, *40*, 1926−36. (h) Degennaro, L.; Trinchera, P.; Luisi, R. *Chem. Rev.* **2014**, *114*, 7881−7929.

(4) For selected reviews of Rh-catalyzed nitrene transfer, see: (a) Roizen, J. L.; Harvey, M. E.; Du Bois, J. *Acc. Chem. Res.* **2012**, *45*, 911−22. (b) Collet, F.; Lescot, C.; Liang, C. G.; Dauban, P. *Dalton Trans.* **2010**, *39*, 10401−13. For Ag, see: (c) Gómez-Emeterio, B. P.; Urbano, J.; Díaz-Requejo, M. M.; Pérez, P. J. *Organometallics* **2008**, *27*, 4126−30. (d) Kornecki, K. P.; Berry, J. F. *Chem. - Eur. J.* **2011**, *17*, 5827−32.

(5) For selected examples of Ag-catalyzed nitrene transfer, see: (a) Cui, Y.; He, C. *J. Am. Chem. Soc.* **2003**, *125*, 16202−03. (b) Cui, Y.; He, C. *Angew. Chem., Int. Ed.* **2004**, *43*, 4210−12. (c) Li, Z.; Capretto, D. A.; Rahaman, R. H.; He, C. *Angew. Chem., Int. Ed.* **2007**, *46*, 5184−86. (d) Llaveria, J.; Beltran, A.; Diaz-Requejo, M. M.; Matheu, M. I.; Castillon, S.; Perez, P. J. *Angew. Chem., Int. Ed.* **2010**, *49*, 7092−95.

(6) For an example of Co/Pd-catalyzed nitrene transfer, see: Huang, G. − H.; Li, J.-M.; Huang, J.-J.; Lin, J.-D.; Chuang, G. J. *Chem. - Eur. J.* **2014**, *20*, 5240−43.

(7) For selected examples of Ru-catalyzed nitrene transfer, see: (a) Au, S.-M.; Fung, W.-H.; Cheng, M.-C.; Che, C.-M.; Peng, S.-M. *Chem. Commun.* **1997**, 1655−58. (b) Au, S.-M.; Huang, J.-S.; Che, C.-M.; Yu, W.-Y. *J. Org. Chem.* **2000**, *65*, 7858−64.

(8) For selected examples of Cu-catalyzed nitrene transfer, see: (a) Evans, D. A.; Faul, M. M.; Bilodeau, M. T. *J. Org. Chem.* **1991**, *56*, 6744−46. (b) Evans, D. A.; Faul, M. M.; Bilodeau, M. T. *J. Am. Chem. Soc.* **1994**, *116*, 2742−53. (c) Dielmann, F.; Andrada, D. M.; Frenking, G.; Bertrand, G. *J. Am. Chem. Soc.* **2014**, *136*, 3800−02.

(9) For selected references on Co-catalyzed nitrene transfer, see: (a) Lu, H. J.; Subbarayan, V.; Tao, J. R.; Zhang, X. P. *Organometallics* **2010**, *29*, 389−393. (b) Lu, H.-J.; Jiang, H.-L.; Hu, Y.; Wojtas, L.; Zhang, X. P. *Org. Lett.* **2012**, *14*, 5158−5161. (c) Lu, H.-J.; Jiang, H.-L.; Hu, Y.; Wojtas, L.; Zhang, X. P. *Chem. Sci.* **2011**, *2*, 2361−2366. (d) Lu, H.-J.; Jiang, H.-L.; Wojtas, L.; Zhang, X. P. *Angew. Chem., Int. Ed.* **2010**, *49*, 10192−10196. (e) Lu, H.-J.; Li, C.-Q.; Jiang, H.-L.; Lizardi, C. L.; Zhang, X. P. *Angew. Chem., Int. Ed.* **2014**, *53*, 7028−7032.

(10) For examples with Fe, see: (a) Kuppuswamy, S.; Powers, T. M.; Johnson, B. M.; Bezpalko, M. W.; Brozek, C. K.; Foxman, B. M.; Berben, L. A.; Thomas, C. M. *Inorg. Chem.* **2013**, *52*, 4802−11. (b) King, E. R.; Hennesy, E. T.; Betley, T. A. *J. Am. Chem. Soc.* **2011**, *133*, 4917−4923. (c) Bowman, A. C.; Milsmann, C.; Bill, E.; Turner, Z. R.; Lobkovsky, E.; DeBeer, S.; Wieghardt, K.; Chirik, P. J. *J. Am. Chem. Soc.* **2011**, *133*, 17353−69. For Ru, see: (d) Takaoka, A.; Moret, M.-E.; Peters, J. C. *J. Am. Chem. Soc.* **2012**, *134*, 6695−6703. (e) Takaoka, A.; Gerber, L. C. H.; Peters, J. C. *Angew. Chem., Int. Ed.* **2010**, *49*, 4088−91. (f) Fantauzzi, S.; Gallo, E.; Ragaini, F.; Casati, N.; Macchi, P.; Cenini, S. *Chem. Commun.* **2009**, 3952−3954. For Co, see: (g) King, E. R.; Sazama, G. T.; Betley, T. A. *J. Am. Chem. Soc.* **2012**, *134*, 17858−61. (h) Jones, C.; Schulten, C.; Rose, R. P.; Stasch, A.; Aldridge, S.; Woodul, W. D.; Murray, K. S.; Moubaraki, B.; Brynda, M.; Macchia, G. L.; Gagliardi, L. *Angew. Chem., Int. Ed.* **2009**, *48*, 7406−7410.

(11) (a) Hayes, C. J.; Beavis, P. W.; Humphries, L. A. *Chem. Commun.* **2006**, 4501−2. (b) Fiori, K. W.; Du Bois, J. *J. Am. Chem. Soc.* **2007**, *129*, 562−68. (c) Zalatan, D. N.; Du Bois, J. *J. Am. Chem. Soc.* **2008**, *130*, 9220−21. (d) Kornecki, K. P.; Berry, J. F. *Eur. J. Inorg. Chem.* **2012**, *2012*, 562−568. (e) Cramer, S. A.; Jenkins, D. M. *J. Am. Chem. Soc.* **2011**, *133*, 19342−45. (f) Hennessy, E. T.; Liu, R. Y.; Iovan, D. A.; Duncan, R. A.; Betley, T. A. *J. Am. Chem. Soc.* **2014**, *5*, 1526−9. (g) Srivastava, R. S.; Tarver, N. R.; Nicholas, K. M. *J. Am. Chem. Soc.* **2007**, *129*, 15250−58. (h) Barman, D. N.; Nicholas, K. M. *Eur. J. Org. Chem.* **2011**, *2011*, 908−911.

(12) (a) Harvey, M. E.; Musaev, D. G.; Du Bois, J. *J. Am. Chem. Soc.* **2011**, *133*, 17207−16. (b) Paradine, S. M.; White, M. C. *J. Am. Chem. Soc.* **2012**, *134*, 2036−9. (c) Paradine, S. M.; Griffin, J. R.; Zhao, J.; Petronico, A. L.; Miller, S. M.; White, M. C. *Nat. Chem.* **2015**, *7*, 987−994.

(13) (a) Alderson, J. A.; Phelps, A. M.; Scamp, R. J.; Dolan, N. S.; Schomaker, J. M. *J. Am. Chem. Soc.* **2014**, *136*, 16720−3. (b) Rigoli, J. W.; Weatherly, C. D.; Alderson, J. M.; Vo, B. T.; Schomaker, J. M. *J.*

DOI: 10.1021/acs.organomet.7b00190
Organometallics XXXX, XXX, XXX−XXX

Am. Chem. Soc. **2013**, *135*, 17238−41. (c) Rigoli, J. W.; Weatherly, C. D.; Vo, V. T.; Neale, S.; Meis, A. R.; Schomaker, J. M. *Org. Lett.* **2013**, *15*, 290−3. (d) Scamp, R. J.; Rigoli, J. W.; Schomaker, J. M. *Pure Appl. Chem.* **2014**, *86*, 381−393.

(14) (a) Hung-Low, F.; Renz, A.; Klausmeyer, K. K. *Polyhedron* **2009**, *28*, 407−15. (b) Hung-Low, F.; Renz, A.; Klausmeyer, K. K. *J. Chem. Crystallogr.* **2011**, *41*, 1174−79. (c) Du, J.; Hu, T.; Zhang, S.; Zeng, Y.; Bu, X. *CrystEngComm* **2008**, *10*, 1866−74. (d) Zhang, H.; Chen, L.; Song, H.; Zi, G. *Inorg. Chim. Acta* **2011**, *366*, 320−36. (e) Hung-Low, F.; Renz, A.; Klausmeyer, K. K. *J. Chem. Crystallogr.* **2009**, *39*, 438−44. (f) Levason, W.; Spicer, M. D. *Coord. Chem. Rev.* **1987**, *76*, 45−120. (g) Leschke, M.; Rheinwald, G.; Lang, H. *Z. Anorg. Allg. Chem.* **2002**, *628*, 2470−77. (h) Zhu, H.-L.; Chen, Q.; Peng, W.-l.; Qi, S.-J.; Xu, S.-J.; Xu, A.-L.; Chen, X.-M. *Chin. J. Chem.* **2001**, *19*, 263−267. (i) Bowmaker, G. A.; Effendy; Marfuah, S.; Skelton, B. W.; White, A. H. *Inorg. Chim. Acta* **2005**, *358*, 4371−88. (j) Paramonov, S. E.; Kozmina, N. O.; Stroganov, S. I. *Polyhedron* **2003**, *22*, 837−841. (k) Han, Z.; Wang, Y.; Wu, J.; Zhai, X. *Solid State Sci.* **2011**, *13*, 1560−1566. (l) Yuan, L.; Qin, C.; Wang, X.; Li, Y.; Wang, E. *Dalton Trans.* **2009**, 4169−75. (m) Pang, H.-J.; Chen, J.; Peng, J.; Sha, J.-Q.; Shi, Z.-Y.; Tian, A.-X.; Zhang, P.-P. *Solid State Sci.* **2009**, *11*, 824−828.

(15) (a) Nageli, I.; Baud, C.; Bernardinelli, G.; Jacquier, Y.; Moran, M.; Muller, P. *Helv. Chim. Acta* **1997**, *80*, 1087−1105. (b) Muller, P.; Baud, C.; Nageli, I. *J. Phys. Org. Chem.* **1998**, *11*, 597−601. (c) Au, S.-M.; Huang, J.-S.; Yu, W.-Y.; Che, C.-M. *J. Am. Chem. Soc.* **1999**, *121*, 9120−9132. (d) Liang, J.-L.; Yuan, S.-X.; Huang, J.-S.; Che, C.-M. *J. Org. Chem.* **2004**, *69*, 3610−19. (e) Leung, S. K. − Y.; Tsui, W.-M.; Huang, J.-S.; Che, C.-M.; Leung, J.-L.; Zhu, N. *J. Am. Chem. Soc.* **2005**, *127*, 16629−16640. (f) Badiei, Y. M.; Krishnaswamy, A.; Melzer, M. M.; Warren, T. H. *J. Am. Chem. Soc.* **2006**, *128*, 15056−7. (g) Huard, K.; Lebel, H. *Chem. - Eur. J.* **2008**, *14*, 6222−30. (h) Maestre, L.; Sameera, W. M.; Díaz-Requejo, M. M.; Maseras, F.; Perez, P. J. *J. Am. Chem. Soc.* **2013**, *135*, 1338−48. (i) Aguila, M. J. B.; Badiei, Y. M.; Warren, T. H. *J. Am. Chem. Soc.* **2013**, *135*, 9399−9406. (j) Fiori, K. W.; Espino, C. G.; Brodsky, B. H.; Du Bois, J. *Tetrahedron* **2009**, *65*, 3042−51. (k) Lyaskovskyy, V.; Suarez, A. I. O.; Lu, H.; Jiang, H.; Zhang, X. P.; de Bruin, B. *J. Am. Chem. Soc.* **2011**, *133*, 12264−73. (l) Li, Z.; Quan, R. W.; Jacobsen, E. N. *J. Am. Chem. Soc.* **1995**, *117*, 5889−90. (m) Han, H.; Park, S. B.; Kim, S. K.; Chang, S. *J. Org. Chem.* **2008**, *73*, 2862−2870. (n) Lebel, H.; Lectard, S.; Parmentier, M. *Org. Lett.* **2007**, *9*, 4797−4800.

(16) Kwart, H.; Khan, A. A. *J. Am. Chem. Soc.* **1967**, *89*, 1951−53.

(17) (a) Zhang, X.; Ke, Z.; DeYonker, N. J.; Xu, H.; Li, Z.-F.; Xu, X.; Zhang, X.; Su, C.-Y.; Phillips, D. L.; Zhao, C. *J. Org. Chem.* **2013**, *78*, 12460−68. (b) Liu, Y.; Guan, X.; Wong, E. L.-M.; Liu, P.; Huang, J.-S.; Che, C.-M. *J. Am. Chem. Soc.* **2013**, *135*, 7194−7204.

(18) (a) Zhang, X.; Xu, H.; Zhao, C. *J. Org. Chem.* **2014**, *79*, 9799−9811. (b) Varela-Álvarez, A.; Yang, T.; Jennings, H.; Kornecki, K. P.; Macmillan, S. N.; Lancaster, K. M.; Mack, J. B. C.; Du Bois, J.; Berry, J. F.; Musaev, D. G. *J. Am. Chem. Soc.* **2016**, *138*, 2327−2341.

(19) (a) Lin, X.; Zhao, C.; Che, C.-M.; Ke, Z.; Phillips, D. L. *Chem. - Asian J.* **2007**, *2*, 1101−8. (b) Barman, D. N.; Liu, P.; Houk, K. N.; Nicholas, K. M. *Organometallics* **2010**, *29*, 3404−12. (c) Lin, X.; Xi, Y.; Sun, J. *Comput. Theor. Chem.* **2012**, *999*, 74−82.

(20) Newcomb, M.; Johnson, C. C.; Manek, M. B.; Varick, T. R. *J. Am. Chem. Soc.* **1992**, *114*, 10915−21.

(21) While Hammett studies of aziridination can also yield valuable mechanistic information, substrate styrenes bearing a two-carbon tether between alkene and carbamates gave primarily C−H amination under the standard aziridination conditions. Substrates bearing a one-carbon tether are known to undergo aziridination in the absence of a catalyst. See: Deng, Q.-H.; Wang, J.-C.; Xu, J.-J.; Zhou, C.-Y.; Che, C.-M. *Synthesis* **2011**, *2011*, 2959−2967.

(22) Hansch, C.; Leo, A.; Taft, R. W. *Chem. Rev.* **1991**, *91*, 165−95.

(23) Jiang, X.-K.; Ji, G.-Z. *J. Org. Chem.* **1992**, *57*, 6051−56.

(24) When only the σ^+ term was considered, as in the Du Bois study, a ρ value of −0.41 was calculated.

(25) Dolan, N. S.; Scamp, R. J.; Yang, T.; Berry, J. F.; Schomaker, J. M. *J. Am. Chem. Soc.* **2016**, *138*, 14658−14667.

(26) (a) Kundu, S.; Miceli, E.; Farquhar, E.; Pfaff, F. F.; Kuhlmann, U.; Hildebrandt, P.; Braun, B.; Greco, C.; Ray, K. *J. Am. Chem. Soc.* **2012**, *134*, 14710−14713. (b) Badiei, Y. M.; Dinescu, A.; Dai, X.; Palomino, R. M.; Heinemann, F. W.; Cundari, T. R.; Warren, T. H. *Angew. Chem., Int. Ed.* **2008**, *47*, 9961−4.

(27) Fischer, T.; Zabel, M.; Yersin, H.; Monkowius, U. *Acta Crystallogr., Sect. E: Struct. Rep. Online* **2007**, *63*, M2364.

(28) Pucci, D.; Crispini, A.; Ghedini, M.; Szerb, E. I.; La Deda, M. *Dalton Trans.* **2011**, *40*, 4614−4622.

(29) Berry, J. F.; Bill, E.; Garcia-Serres, R.; Neese, F.; Weyhermuller, T.; Wieghardt, K. *Inorg. Chem.* **2006**, *45*, 2027−37.

(30) Ganzenmuller, G.; Berkaine, N.; Fouqueau, A.; Casida, M. E.; Reiher, M. *J. Chem. Phys.* **2005**, *122*, 234321.

(31) Ganzenmuller, G.; Casida, M. E.; Daku, L. M. L.; Hauser, A.; Neese, F. *J. Chem. Phys.* **2005**, *122*, 234321.

(32) Fouqueau, A.; Mer, S.; Casida, M. E.; Daku, L. M. L.; Hauser, A.; Mineva, T.; Neese, F. *J. Chem. Phys.* **2004**, *120*, 9473−9486.

(33) (a) Blackmond, D. G. *Angew. Chem., Int. Ed.* **2005**, *44*, 4302−20. (b) Hein, J. E.; Armstrong, A.; Blackmond, D. G. *Org. Lett.* **2011**, *13*, 4300−4303. (c) Blackmond, D. G. *J. Am. Chem. Soc.* **2015**, *137*, 10852−10866.

(34) Burés, J. *Angew. Chem., Int. Ed.* **2016**, *55*, 2028−31.

(35) (a) Rosner, T.; Le Bars, J.; Pfaltz, A.; Blackmond, D. G. *J. Am. Chem. Soc.* **2001**, *123*, 1848−1855. (b) F. van Strijdonck, G. P.; Boele, M. D. K.; Kamer, P. C. J.; de Vries, J. G.; van Leeuwen, P. W. N. M. *Eur. J. Inorg. Chem.* **1999**, *1999*, 1073−1076.

(36) Fischer, T.; Zabel, M.; Yersin, H.; Monkowius, U. *Acta Crystallogr., Sect. E: Struct. Rep. Online* **2007**, *63*, M2364.

(37) Pucci, D.; Crispini, A.; Ghedini, M.; Szerb, E. I.; La Deda, M. *Dalton Trans.* **2011**, *40*, 4614−4622.

(38) *Avogadro, 1.1.0 edition*.

(39) Neese, F.; Becker, U.; Ganyushin, D.; Hansen, A.; Liakos, D.; Izsak, R.; Kollmar, C.; Petrenko, T.; Riemann, C.; Roemelt, M.; Riplinger, C.; Sandhoefer, B.; Schapiro, I.; Sivalingam, K.; Wezisla, B.; Wennmohs, F. *ORCA-An ab initio, Density Functional and Semi-empirical Program Package. 2.9.1 ed.*: Muelheim an der Ruhr, Germany, 2012.

(40) Perdew, J. P. *Phys. Rev. B: Condens. Matter Mater. Phys.* **1986**, *33*, 8822−8824.

(41) Becke, A. D. *Phys. Rev. A: At., Mol., Opt. Phys.* **1988**, *38*, 3098−3100.

(42) Schafer, A.; Horn, H.; Ahlrichs, R. *J. Chem. Phys.* **1992**, *97*, 2571−2577.

(43) Weigend, F.; Ahlrichs, R. *Phys. Chem. Chem. Phys.* **2005**, *7*, 3297−3305.

(44) The Ahlrichs (2d,2p) polarization functions were obtained from the TurboMole basis set library at http://www.turbomole.com/.

(45) Klamt, A.; Schuurmann, G. *J. Chem. Soc., Perkin Trans. 2* **1993**, 799−805.

DOI: 10.1021/acs.organomet.7b00190
Organometallics XXXX, XXX, XXX−XXX